NASA TECHNICAL REPORT

NASA TR R-435

NASA TR R-435

MAGNETOGASDYNAMIC COMPRESSION OF A COAXIAL PLASMA ACCELERATOR FLOW FOR MICROMETEOROID SIMULATION

by E. B. Igenbergs and E. L. Shriver

George C. Marshall Space Flight Center
Marshall Space Flight Center, Ala. 35812

NATIONAL AERONAUTICS AND SPACE ADMINISTRATION • WASHINGTON, D. C. • OCTOBER 1974

1 REPORT NO.	2. GOVERNMENT ACCESSION NO.	3 RECIPIENT'S CATALOG NO.
NASA TR R-435		

4 TITLE AND SUBTITLE	5. REPORT DATE
Magnetogasdynamic Compression of a Coaxial Plasma Accelerator Flow for Micrometeoroid Simulation	October 1974
	6 PERFORMING ORGANIZATION CODE

7 AUTHOR(S)	8 PERFORMING ORGANIZATION REPORT #
E B. Igenbergs* and E L. Shriver	M465

9 PERFORMING ORGANIZATION NAME AND ADDRESS	10. WORK UNIT NO.
George C. Marshall Space Flight Center Marshall Space Flight Center, Alabama 35812	11. CONTRACT OR GRANT NO.
	13. TYPE OF REPORT & PERIOD COVERED
12. SPONSORING AGENCY NAME AND ADDRESS	
National Aeronautics and Space Administration Washington, D.C 20546	Technical Report
	14. SPONSORING AGENCY CODE

15. SUPPLEMENTARY NOTES

Prepared by Space Sciences Laboratory, Science and Engineering

*Formerly NAS, NRC Postdoctoral Research Associate, now at the Technische Universität München, Germany

16. ABSTRACT

A new configuration of a coaxial plasma accelerator with self-energized magnetic compressor coil attached is described. It is shown that the circuit may be treated theoretically by analyzing an equivalent circuit mesh. The results obtained from the theoretical analysis compare favorably with the results measured experimentally

Using this accelerator configuration, glass beads of 125 micron diameter were accelerated to velocities as high as 11 kilometers per second, while 700 micron diameter glass beads were accelerated to velocities as high as 5 kilometers per second. The velocities are within the hypervelocity regime of meteoroids.

17 KEY WORDS	18. DISTRIBUTION STATEMENT
	CAT. 25

19 SECURITY CLASSIF. (of this report)	20. SECURITY CLASSIF. (of this page)	21. NO. OF PAGES	22 PRICE
Unclassified	Unclassified	64	$3.75

For sale by National Technical Information Service, Springfield, Virginia 22151

ACKNOWLEDGMENTS

The authors wish to thank Mr. Burton Cour-Palais of the Johnson Space Center for his assistance in instrumentation and data acquisition and Dr. Francis C. Todd of the University of Alabama, Huntsville, for his encouragement and for his valuable discussions The authors also received encouragement and help from Dr. R J. Naumann, Mr. Elmer Fisher, and others at the George C Marshall Space Flight Center and thank them for their contributions, and Professor Dr. Harry O. Ruppe of the Technische Universität Munchen for his support of the theoretical investigations.

TABLE OF CONTENTS

		Page
I.	INTRODUCTION	1
II.	DESCRIPTION OF THE PLASMA HYPERVELOCITY ACCELERATOR	2
	A. Capacitor Bank and Switch Assembly	2
	B. Test Range with Plasma Accelerator	2
	C. Diagnostics and Particle Velocity Measurement	3
III.	PLASMA COMPRESSION AND PARTICLE ACCELERATION	7
	A. Drag Acceleration of Particles for Micrometeoroid Simulation	7
	B. Coaxial Accelerator for Particle Acceleration	10
	C. Compressor Coil Configuration	13
IV.	THEORETICAL INVESTIGATION	16
	A. The Equivalent Circuit	16
	B. Analytical Solution for a Simplified Case	20
	C Numerical Integration of the Equations for the Equivalent Circuit	23
V.	EXPERIMENTAL AND THEORETICAL RESULTS	30
	A. Plasma Flow	30
	B. Particle Acceleration	39
VI	DESCRIPTION OF THE COMPUTER PROGRAM	41
	A. Input Data	43
	B. Integration	43
	C. Example of Calculations	44
VII	CONCLUSION	46
APPENDIX	COMPUTER PROGRAM LISTING	49
REFERENCES		57

LIST OF ILLUSTRATIONS

Figure	Title	Page
1	Schematic diagram of plasma hypervelocity range	3
2.	Test range with plasma accelerator	5
3.	Coaxial accelerator with compressor coil	5
4.	Drum probe for impulse measurement	8
5.	Plasma leaving the coaxial accelerator	11
6.	Particle acceleration near center electrode of coaxial accelerator	12
7.	Description of secondary discharge between center electrode and copper ring	12
8.	Photograph of secondary discharge	13
9	Compressor coil with magnetic field and plasma current density	14
10.	Photograph of plasma flow in compressor coil during compression period	14
11.	Equivalent circuit for coaxial accelerator with compressor coil	17
12	Compressor coil current from equation (44)	23
13.	Plasma velocity at the end of the coaxial accelerator	32
14.	Time of arrival of the plasma at the compressor coil	33
15.	Capacitor bank voltage	35
16.	Compressor coil current	35
17	Coaxial accelerator current	39
18	Photograph of accelerated particles in compressor coil plasma flow	40
19.	Particle velocity as function of capacitor bank charging voltage	41

LIST OF ILLUSTRATIONS (Concluded)

Figure	Title	Page
20	Particle velocity as function of the particle initial diameter	42
21.	Voltage and current curves for different values of the constant K7 . .	45
22.	Voltage and current curves for different values of the plasma resistance X5	47

LIST OF TABLES

Table	Title	Page
1	Physical Characteristics of Equipment in Coaxial Accelerator Circuit	4
2	Measured Data for Test Facility	9
3.	Experimental and Theoretical Data	34

MAGNETOGASDYNAMIC COMPRESSION OF A COAXIAL PLASMA ACCELERATOR FLOW FOR MICROMETEOROID SIMULATION

I. INTRODUCTION

The extended duration of manned space flight missions and unmanned operations with very sensitive equipment makes it necessary to provide an adequate protection against micrometeoroid impact Experimental work on the meteoroid impact problem is performed using several types of projectile accelerators which provide high velocity simulated micrometeoroid fluxes in the laboratory

The light gas gun is the most commonly used tool. It accelerates metallic and nonmetallic particles with diameters from 0 015 cm to 0.635 cm to velocities as high as 9.5 km/s, and the maximum particle energy is about $1\,4 \times 10^3$ J (0 316 cm diameter lexan cylinder at 9.5 km/s) [1,2]. More recently, detonation waves in explosives have been used to generate a high speed gas flow [3] which is used to accelerate a projectile For small particle diameters, 1 micron and below, electrostatic accelerators are very useful and reliable micrometeoroid flux simulators [4,5] The energy of the accelerated particles is limited by the charge-to-mass ratio Very small particles with diameters of about 0 1 micron can be accelerated to velocities of approximately 70 km/s. Several efforts have been made to transfer the energy stored in a capacitor bank to particles for micrometeoroid simulation The most successful accelerator has been developed by Scully [6] His device can accelerate particles with diameters of approximately 50 microns to velocities of about 20 km/s.

The experimental and theoretical investigations described in the subsequent sections of this report were aimed at the development of a new concept for the generation of a high density plasma for particle acceleration The energy stored in a capacitor bank is used to generate a high velocity, hot plasma in a coaxial accelerator [7,8,9,10,11] The plasma leaving the coaxial accelerator is compressed in a compressor coil which is mounted on the exit end of the accelerator The most interesting feature of this new combination of coaxial accelerator and compressor coil is that the compressor coil does not need an external power source It obtains the energy needed to compress the plasma from the capacitor bank which is discharged across the coaxial accelerator The new device is, therefore, very simple and can be added easily to existing coaxial plasma accelerators It has been demonstrated that glass beads of 125 to 700 micron diameter can be accelerated to velocities of 11 km/s to 5 km/s, respectively The accelerator configuration is presently being investigated to determine the optimum performance criteria

II. DESCRIPTION OF THE PLASMA HYPERVELOCITY ACCELERATOR

The plasma hypervelocity range for micrometeoroid simulation at the George C Marshall Space Flight Center's Space Sciences Laboratory consists of a capacitor bank with switch assembly, the test range with plasma accelerator, and installations for plasma diagnostics and particle velocity measurement

A. Capacitor Bank and Switch Assembly

The capacitor bank consists of 72 individual 15-microfarad capacitors connected in parallel in groups of 18 capacitors All of the experiments were made with only one quarter bank The maximum charge voltage was 20 kV and the corresponding stored energy was 54 kJ. Three capacitors connected in parallel by copper bus bars form a module, and every module is connected to the switch assembly by two coaxial cables All the cables are the same length. Each quarter bank is equipped with four ignitron switches in parallel. These are fired by a trigger assembly containing a set of capacitors and a thyratron to prevent back current to the igniters of the ignitrons. The switch assembly is connected to the coaxial accelerator by six coaxial cables.

The capacitor bank is charged from a high voltage supply which is controlled by an autotransformer and is disconnected before firing For emergencies a dump circuit is incorporated to discharge any energy stored in the capacitor bank through the charging network within 30 seconds at a peak current of 4 microamps If a prefire occurs, the relays connecting the high voltage power supply and the capacitor bank become de-energized The trigger assembly has its own high voltage power supply and is charged to 5 kV It is activated by a 150-V pulse from a delay generator which, in turn, is triggered either by an external input or manually A schematic diagram of the capacitor bank, charging circuit, switch assembly, and test range is shown in Figure 1 Table 1 lists the characteristics of the equipment

B. Test Range with Plasma Accelerator

The test range is made of a 2 0-m long, 15-cm diameter aluminum tube with a flange at both ends (Fig 2) It has one 38- by 12 5-cm window of 2 5-cm thick Plexiglas for photographing the plasma flow and the particle acceleration The inner surface of the window is covered with a 3-mm replaceable Plexiglas cover for protection against the hot plasma. Two other windows on top of the range have 3.5-cm thick aluminum covers with 5 0-cm diameter, vacuum-tight, feed-through plugs A vacuum pump is connected to the range through a flexible hose The coaxial plasma accelerator with compressor coil is mounted in a fiberglass plate which closes the front end of the test range This plate has two vacuum-tight coaxial cable feed-through plugs for the measurement of the compressor coil current The other end of the test range is closed by an aluminum cover with another feed-through plug and a vacuum gage.

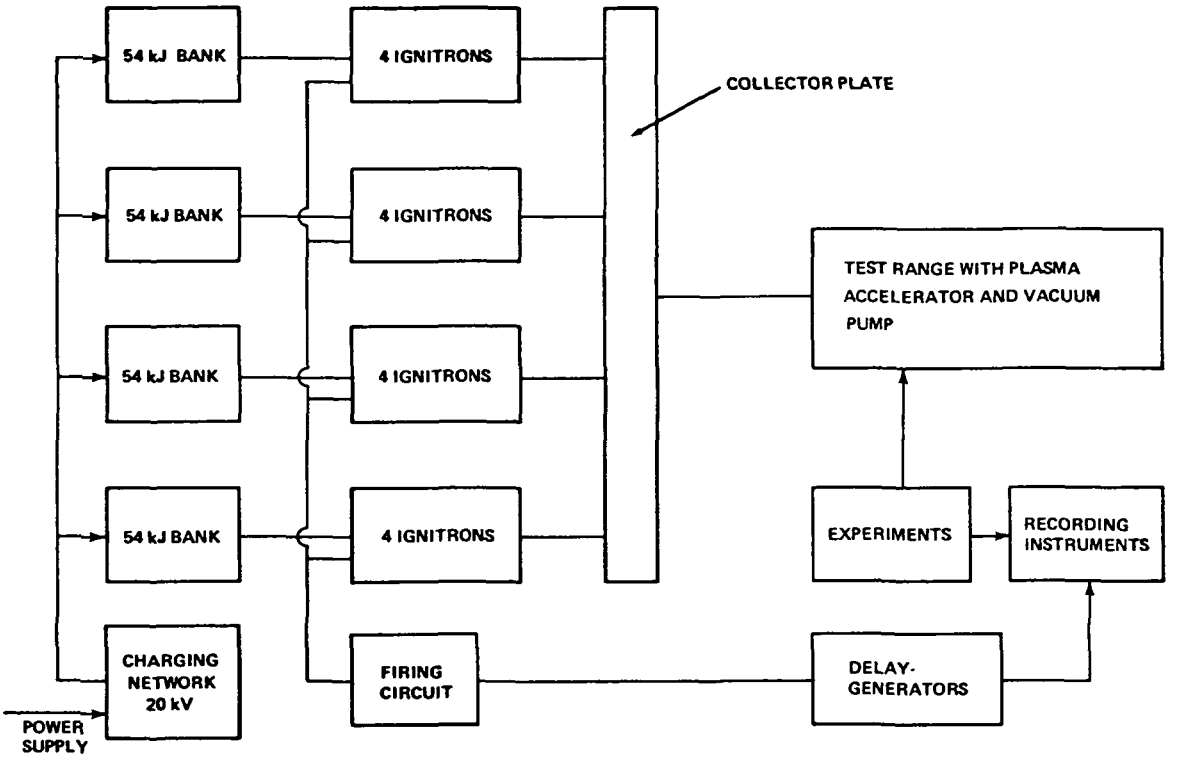

Figure 1 Schematic diagram of plasma hypervelocity range

The coaxial accelerator with compressor coil is shown in Figure 3. The center electrode (1), the insulating plug (2), and the annular electrode (3), form the coaxial accelerator. An aluminum foil (4) is placed between the center electrode and the annular electrode before every firing. The positive side of the charged capacitor bank is connected to the center electrode through the switch assembly, and the negative side is connected to the annular electrode An insulating ring (5) separates the compressor coil (6) from the annular electrode and also serves as a mount The front (narrow) end of the compressor coil is connected to the potential of the annular electrode by the holder rail (7) and is held in position by the coil spacer plate (8) The coil spacer adapter (9) keeps the holder rails in position In the increasing inductance mode configuration, the insulation ring (5) was not used and the holder rail (7) was disconnected from the annular electrode

C. Diagnostics and Particle Velocity Measurement

Photographs of the plasma flow and the accelerated particles were made through the 38- by 12.5-cm window in the range Two single frame image converter cameras were used for high speed photographs They were triggered by the pulse from the delay

generator to the capacitor bank firing circuit Using the adjustable exposure delay of the cameras, the time interval between the two exposures could be set between 0 and 100 microseconds

TABLE 1 PHYSICAL CHARACTERISTICS OF EQUIPMENT IN COAXIAL ACCELERATOR CIRCUIT

Equipment/Characteristic	Description
Capacitors	
Peak dc Voltage Rating	20 kilovolt
Capacitance	15 microfarad +20%-10%
Inductance	40 nanohenry max
Energy	300 joule
Voltage Reversal	90%
Peak Current	2×10^5 ampere (direct short)
Life Expectancy	10^5 discharges
Cables	
Type	20 P 2
Peak Voltage	20 kilovolt
Reversal Level for Full Nominal Life	19 kilovolt
Nominal Life	10^5 pulses
Characteristic Impedance	16 ohms ± 1 ohm
Inductance (at 200 kHz)	105 ± 6 6 nanohenry/meter
Delay	6 56 nanosecond/meter
Normal dc Resistance	
Inner Conductor	0 568 ohm/kilometer
Outer Conductor	3 335 ohm/kilometer
Minimum Bending Radius	12 7 centimeter
Capacitance	407 picofarad/meter
Ignitrons	
Type	GL-7703
Peak Anode Voltage (Forward)	20 kilovolt
Peak Anode Voltage (Reverse)	20 kilovolt
Peak Anode Current for One-Half-Cycle of 20 microsecond	10^5 ampere
Tube Inductance	4×10^{-8} henry
Ionization Time	0 5 microsecond
Ignitor Ratings	
Ignitor Voltage	
Forward Open Circuit	1500 volts min 3000 volts max
Inverse Voltage	5 volts max
Peak Ignitor Current	250 ampere max 200 ampere min
Length of Firing Pulse, Sine Wave	5 microsecond min 10 microsecond max

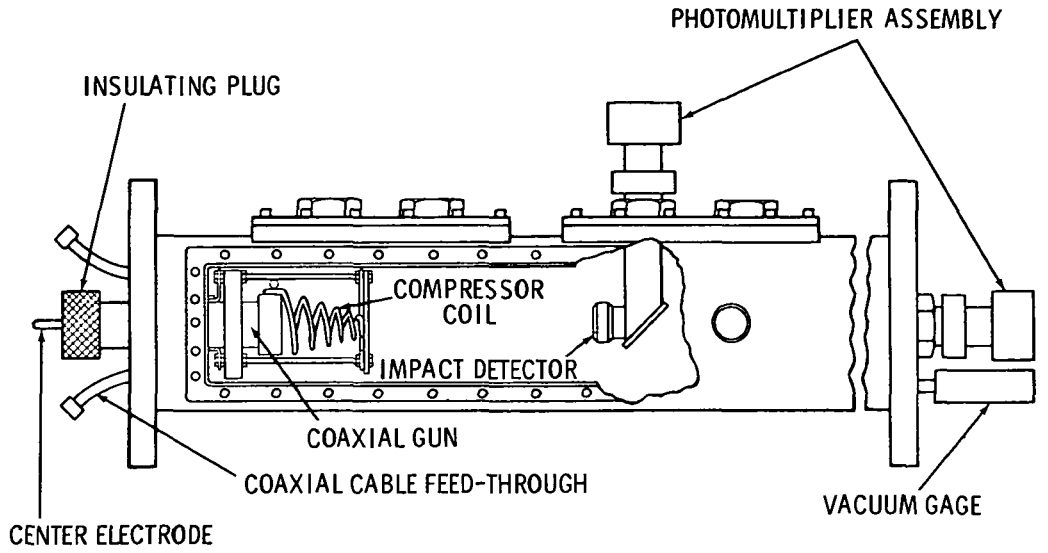

Figure 2 Test range with plasma accelerator.

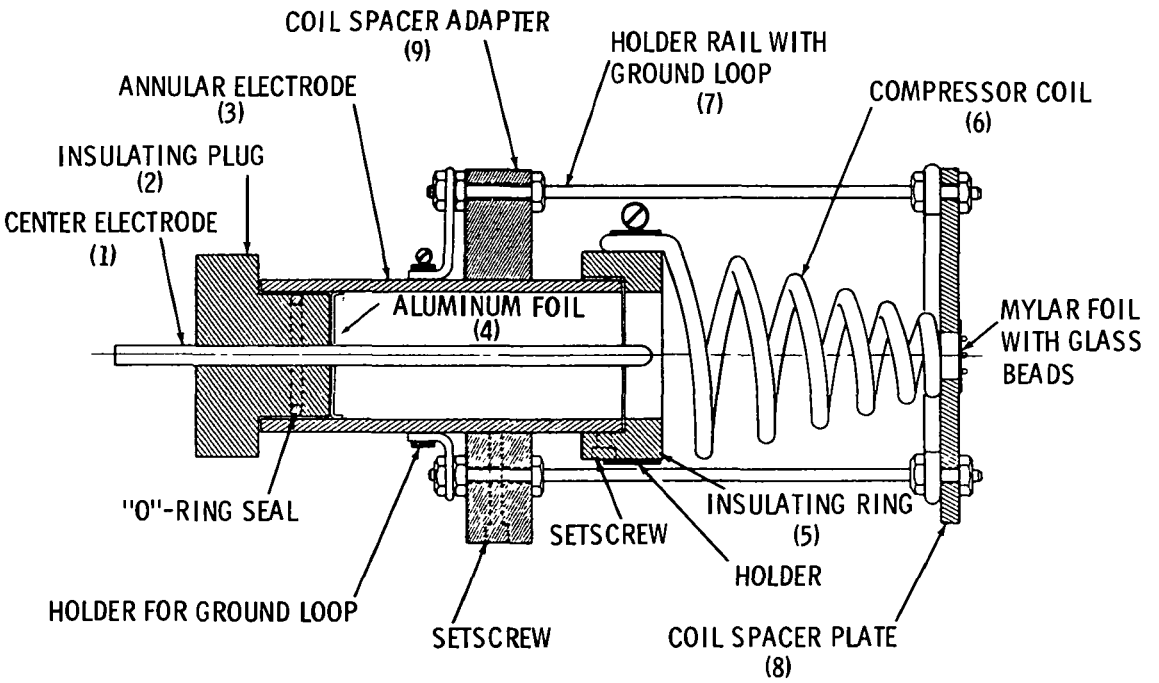

Figure 3. Coaxial accelerator with compressor coil

An eight-camera unit made up of eight individual image converter cameras was used for sequential photographs In this unit the plasma image is deflected by a prism, which is located in the center of a drum-shaped container, to the eight image converter tubes located at 45-deg intervals. For particle detection in the very bright plasma light, filters were placed between the prism in the center and the image converter tubes. The eight cameras could be triggered at a maximum time interval of 1 microsecond between successive frame exposures, whereas, the minimum exposure time was 10 nanoseconds and the maximum exposure time was 100 nanoseconds The trigger pulse for the image converter cameras came from a transient light detector or from the delay generator, which also triggered the capacitor bank firing circuit In both cases, the trigger pulse for the first camera was recorded on an oscilloscope

Light probes were placed in various positions in front of the plasma range window to measure the plasma front propagation velocity The output of these detectors was recorded on an oscilloscope The particle velocity was measured with the eight-camera unit and an impact detector. Using light filters, the particles could be photographed when they left their position at the Mylar foil. The time delays between the eight photographs were recorded on time interval counters. These delay times, together with the recorded trigger pulse for the first camera, bracketed the time when the particles had left their position on the front of the compressor coil

The impact detector (Fig. 2) placed between 0 2 and 0.4 meters downrange had a detector mounted coaxially with the plasma accelerator and compressor coil An aluminum sheet was held in place by a nut The accelerated particles perforated this sheet, and a light flash was generated which was deflected by a mirror into a photomultiplier mounted on the top window cover of the range A hole was punched into one aluminum sheet to determine the origin of the light recorded by the photomultiplier. The plasma light coming through this hole for a discharge with no beads had the same intensity as the signal from a perforation by an accelerated particle It may, therefore, be concluded that the recorded light flash from an aluminum sheet perforation by an accelerated particle is generated by the plasma, either in the accelerator or in a shock wave in front of the impact detector

The output of the photomultiplier detector was recorded on the same dual beam oscilloscope as the trigger pulse for the first camera The particle flight time, together with the known distance between the compressor coil front end where the photographs were made and the aluminum sheet in the particle impact detector, was used to determine the average particle velocity The capacitor bank voltage was measured with an inductive pickup coil mounted on top of the positive leads of the coaxial cables leading from the ignitron switch assembly to the coaxial accelerator The shields of the coaxial cables were stripped from the cables in the switch assembly, the positive leads go through the ignitrons and the shield goes through a ground plate The compressor coil current was measured indirectly by a pickup coil in front of a loop in the backstrap lead from the compressor coil to the center electrode To eliminate electromagnetic disturbances, a second pickup coil was mounted on the other side of the coaxial accelerator to record only the electromagnetic disturbances Both signals were then subtracted in a differential amplifier and then recorded on an oscilloscope

III. PLASMA COMPRESSION AND PARTICLE ACCELERATION

Glass beads with diameters between 0.125 mm and 0.795 mm were used for acceleration experiments There was no indication of any forces other than gasdynamic forces acting upon these beads

A. Drag Acceleration of Particles for Micrometeoroid Simulation

In gasdynamics, the force acting upon a body may be expressed as the sum of a dynamic pressure term and the product of the pressure gradient times a characteristic length ΔZ, both multiplied with a characteristic surface S, which is assumed to be the same here for both terms

$$F = (C_D \frac{\rho}{2} V^2 + \nabla P \Delta Z) S \qquad (1)$$

For constant particle size and flow velocity, V, the dynamic pressure term is only a function of the flow density ρ Plasma accelerators for neutral particle acceleration were, therefore, designed for high flow densities

In a magnetogasdynamic flow the pressure gradient term ∇P may become large if the plasma density is high enough to permit an immediate transfer of the electromagnetic force into gasdynamic pressure Maximum gasdynamic acceleration of neutral particles, therefore, is obtained by high density flow and a large negative pressure gradient. The density of the plasma leaving the coaxial accelerator was measured with the drum probe shown in Figure 4 A metallic foil is attached to a Plexiglas housing The probe in front of the foil indicates the arrival of the electrically conducting plasma, and a current flows between the potential drop across the resistance R1 in Figure 4 The rise-time of the circuit shown in Figure 4 is 1 nanosec/Volt, with the capacitance C in parallel with the battery B. The plasma pushes the foil towards the center electrode. Upon contact, the current through R1 is cut short and the potential drop across R1 becomes zero The time during which a potential can be measured across the resistance R1 is the time during which the foil moves from the initial position to the center electrode.

From the acceleration of the foil with the mass M and the law of the conservation of momentum of the plasma flow hitting the foil, the density ρ of the plasma flow can be calculated Using the data from Table 2, the following value is calculated [7]

$$\rho = 2.5 \times 10^{-2} \text{ kg/m}^3 \qquad (2)$$

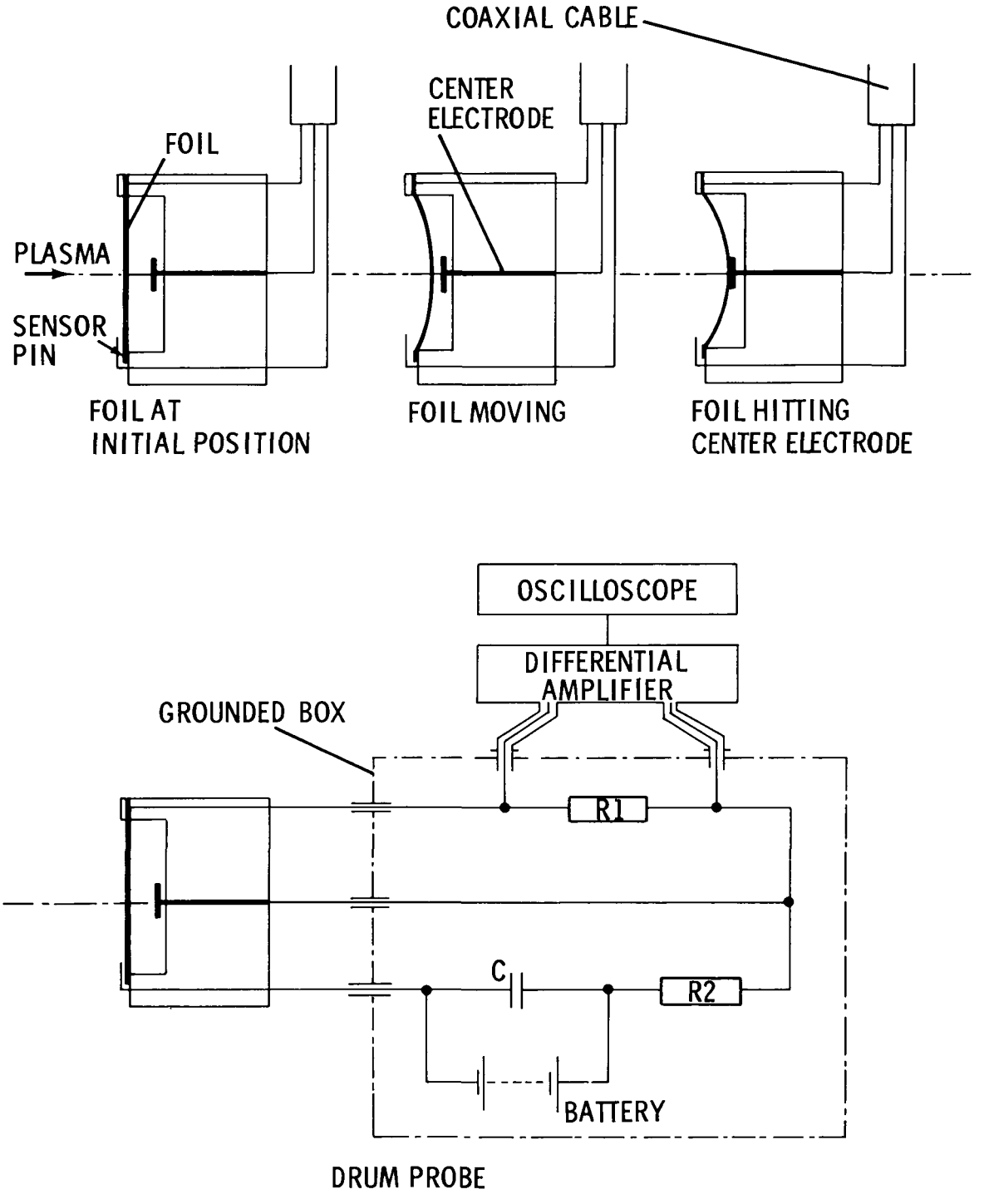

Figure 4 Drum probe for impulse measurement.

TABLE 2. MEASURED DATA FOR TEST FACILITY

Capacitor Bank Charging Voltage	$U_0 = 16$ kV
Initial Pressure in Test Range	$P_0 = 5 \times 10^{-2}$ Torr
Foil Mass	M = 1 0 g
Displacement of Foil	S = 0.35 cm
Foil Radius	R = 1 25 cm
Acceleration Time	$T = 6.0 \times 10^{-6}$ s

Another estimate can be obtained by dividing the mass of the aluminum foil inserted into the coaxial accelerator by the volume of the coaxial accelerator

$$\rho = \frac{M_{FOIL}}{V_{COAX}} = 1\ 06 \times 10^{-1}\ \text{kg/m}^3 \tag{3}$$

A comparison of the results from equations (2) and (3) shows that the measured density is approximately one-fourth of the calculated value This indicates that only a part of the aluminum foil mass is accelerated High-speed photographs using a movie camera show that plasma columns are accelerated at every half-period of the circuit consisting of the capacitor bank, cables, and the coaxial accelerator

The measured density can be introduced into equation (1) Assuming that there is no contribution from the pressure gradient term, the acceleration of a glass bead may be computed using the dynamic term F_D of equation (1),

$$a = \frac{F_D}{M} = \frac{C_D}{2} \left(\frac{\rho_{PLASMA}}{\rho_{GLASS}} \right) \left(\frac{3}{4\ R_{BEAD}} \right) V^2 \tag{4}$$

With the drag coefficient $C_D = 2\ 0$ from the Newtonian approximation for hypersonic flows and the glass density $\rho = 2\ 5$ g/cm^3,

$$a = \frac{3\,V^2}{4\,R} \times 10^{-5}\ \text{m/sec}^2 \tag{5}$$

For V = 40 km/s and R = 0.5 mm, the acceleration is

$$a = 24 \times 10^{7}\ \text{m/sec}^2 \tag{6}$$

Using the measured acceleration time T of the foil for the projectile acceleration, the final velocity of the accelerated glass bead becomes

$$V = a\,T = 144\ \text{m/sec} \tag{7}$$

This result was verified by the experiment No measurable acceleration was obtained when the beads were attached to a Mylar foil and placed across the end of the coaxial accelerator Therefore, an attempt was made to find a region of higher density inside the coaxial accelerator.

B. Coaxial Accelerator for Particle Acceleration

The electromagnetic force in the coaxial accelerator without a compressor coil is generated by the interaction of the radial current density J_r between the center electrode and the annular electrode, and the azimuthal magnetic induction B_ϕ around the center electrode Both are functions of the radial distance r from the center electrode,

$$J_r \sim \frac{1}{r} \qquad \text{and} \qquad B_\phi \sim \frac{1}{r} \tag{8}$$

The axial electromagnetic force is

$$F_Z = J_r\,B_\phi \sim \frac{1}{r^2} \tag{9}$$

and the axial momentum equation becomes

$$\rho \frac{d V_z}{d t} + \frac{\partial P}{\partial z} = F_z \sim \frac{1}{r^2} \quad . \tag{10}$$

The maximum acceleration and pressure gradient will occur in the vicinity of the center electrode. The plasma leaves a coaxial accelerator with equally long center and annular electrodes in a conical shape, as shown in Figure 5. During the acceleration, plasma is forced radially toward the wall of the annular electrode. After 10 to 20 firings, the inner surface of the annular electrode is covered with aluminum deposits. The maximum acceleration of the particles was observed when they were placed near the center electrode, as shown in Figure 6 A copper, ring-shaped holder was inserted into the annular electrode, and the center electrode was shortened If the ring holder is in metallic contact with the annular electrode, then the secondary discharge indicated in Figure 7 occurs. This discharge was photographed with the center electrode protruding out of the annular electrode (Fig. 8). The discharge starts when the plasma fills the gap between the center electrode and the ring holder The azimuthal magnetic field around the discharge interacts with the axial current density and produces a radial force and an axially directed force due to the conical shape of the discharge A thin Mylar foil with glass beads attached to the foil by a thin film of vacuum grease was placed across the ring holder The maximum particle velocity (1.0 to 2.0 km/s with 0.7 mm diameter beads) was achieved with the holder in front of the center electrode inside the annular electrode.

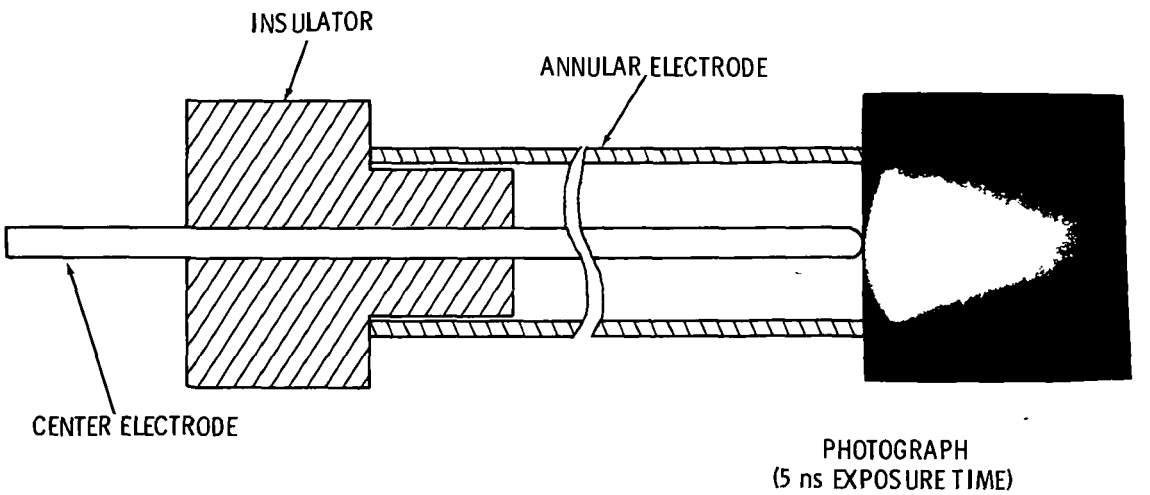

Figure 5 Plasma leaving the coaxial accelerator.

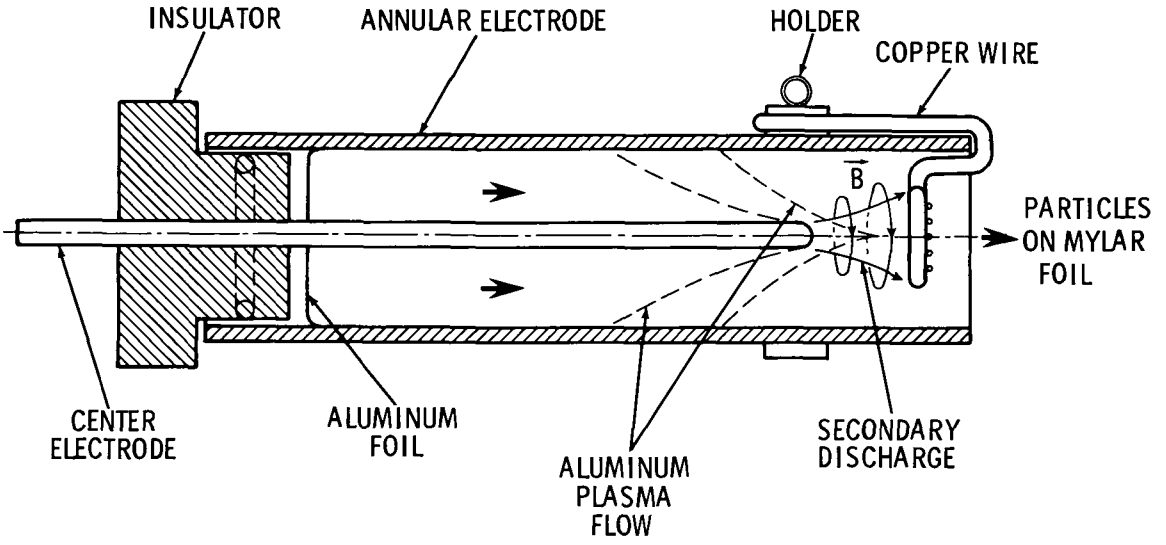

Figure 6. Particle acceleration near center electrode of coaxial accelerator.

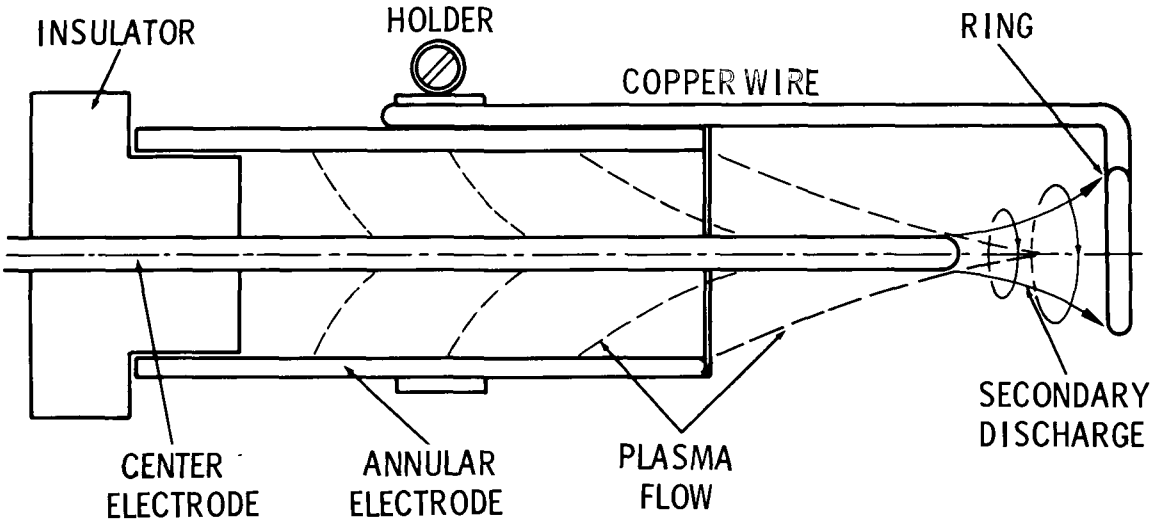

Figure 7. Description of secondary discharge between center electrode and copper ring

It should be noted that the configuration with the center electrode longer than the annular electrode (Fig 7) produced a very high velocity luminous front travelling down the range if no Mylar foil was placed on the ring holder The plasma arrived at the gap between the center electrode and the ring holder with a velocity corresponding to the coaxial accelerator configuration. The secondary-discharge provides additional acceleration

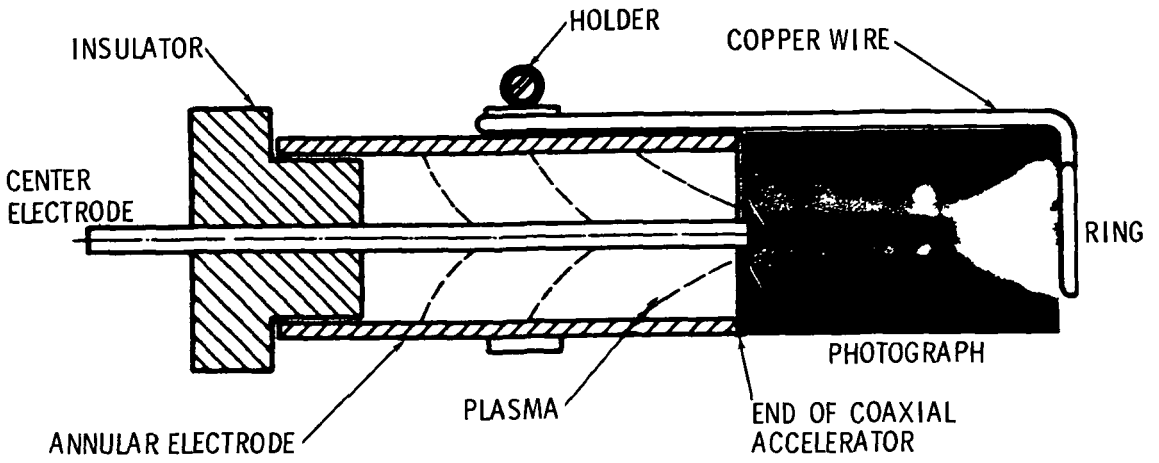

Figure 8 Photograph of secondary discharge

because of its conical geometry and, thus, acts as a second acceleration stage Finally, the coaxial accelerator without the compressor coil produces a fast, low-density plasma The vaporized and ionized aluminum foil does not stay together, and the plasma leaves the accelerator as a column which is at least as long as the accelerator

C. Compressor Coil Configuration

It is more effective to use a compressor coil, as described earlier and shown in Figure 3, mounted on the end of the coaxial accelerator. The emerging plasma initiates a discharge between the center electrode and the copper compressor coil, which is connected to the annular electrode. If the spacing between the coil windings is large enough, then the electric current will flow through the copper coil windings and will generate inside the coil a mostly axial magnetic field (Fig. 9). This magnetic field changes with time and induces an azimuthal current density in the plasma inside the compressor coil which interacts with the magnetic field and results in a radial force on the plasma While the axial magnetic field is increasing, this radial force acts toward the axis, keeping the plasma inside the compressor coil (Fig. 10). The current from the center electrode to the compressor coil has axial and radial components. The azimuthal magnetic field and the radial current density component generate an axial force as in the coaxial accelerator Therefore, the plasma will be compressed and accelerated into the compressor coil at the same time. The current density from the center electrode to the compressor coil is controlled by a local equilibrium between the radial force, which tends to push the plasma away from the compressor coil surface and the current density needed to produce this force

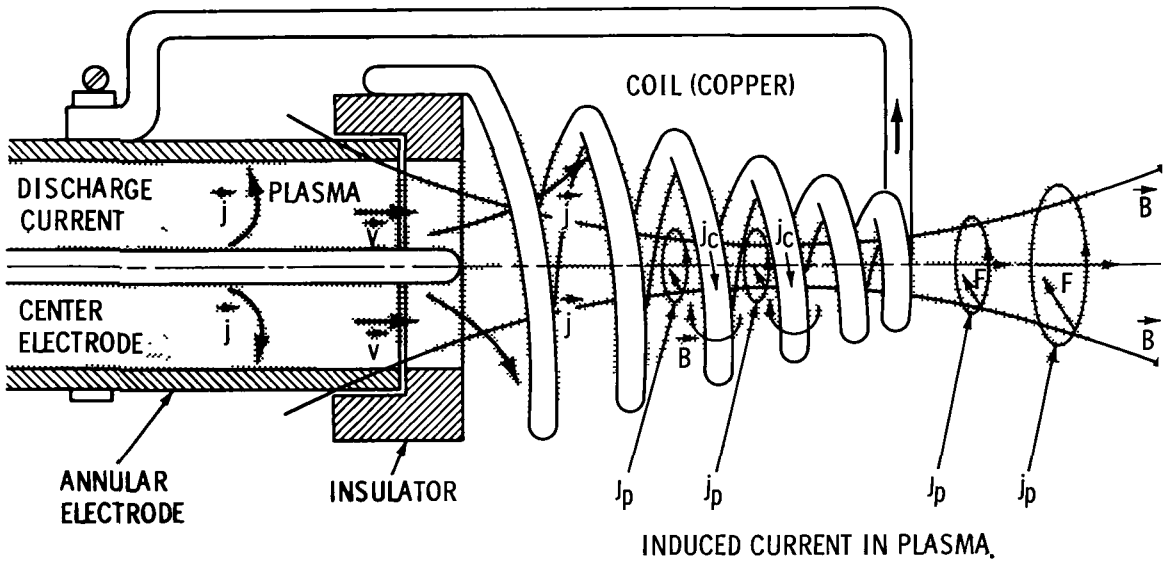

Figure 9. Compressor coil with magnetic field and plasma current density

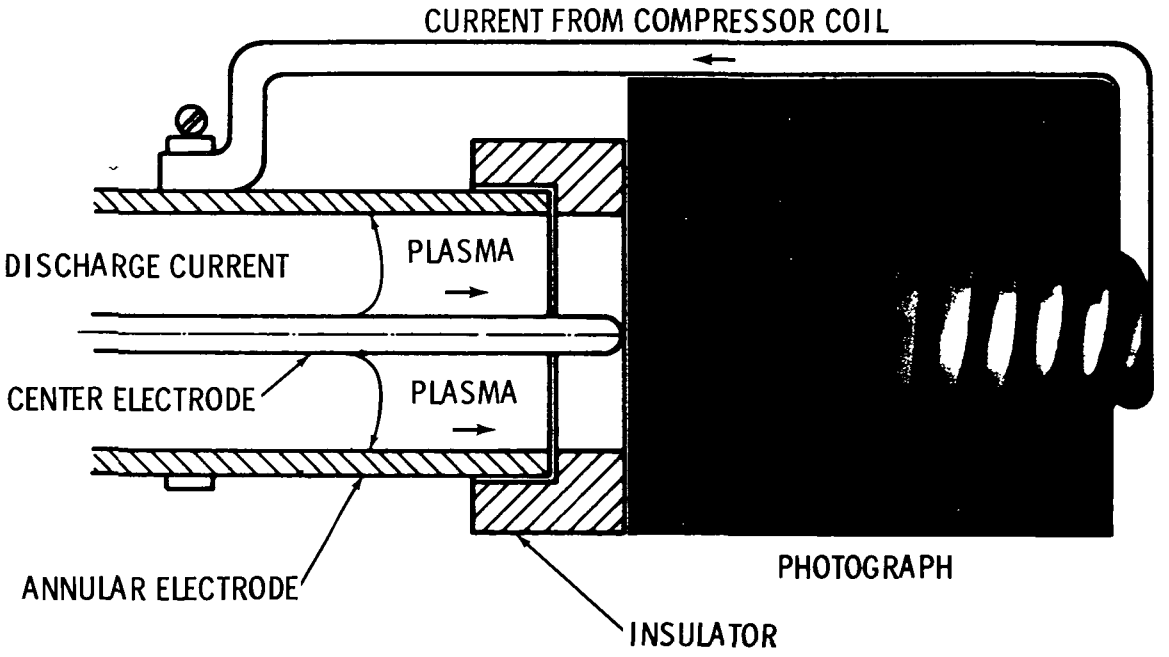

Figure 10 Photograph of plasma flow in compressor coil during compression period.

There are two ways to connect the compressor coil to the annular electrode potential and they lead to two different modes of operation the decreasing and increasing inductance modes. In the decreasing inductance mode, the compressor coil is insulated from the annular electrode by an insulator ring (Fig 3) The end of the compressor coil is connected to the annular electrode through the holder rail As the plasma moves into the compressor coil, the current density will assume some distribution along the compressor coil The current flow to the compressor coil wide end, which is close to the coaxial accelerator end and attached to the insulator ring, will have to traverse all the windings of the compressor coil, whereas the current going to the narrow end of the compressor coil will flow only through the final winding In an equivalent circuit for this configuration every current element must be combined with a different inductance, varying from the total inductance L_1 at the wide end to a small inductance at the narrow end. If $\Delta\ell$ is a length element of the compressor coil, then the position measured from the wide end of the compressor coil is given by $i\Delta\ell$, with i varying from zero to n, where $n\Delta\ell = \ell$, the length of the compressor coil

The inductance L_1 for a current density entering the compressor coil at $i\Delta\ell$ will be

$$L_i = L_1 - i\Delta\ell \frac{L_1}{n\Delta\ell} \tag{11}$$

Then the total inductance L is obtained by adding the different inductances L_i according to the rule for parallel circuits,

$$\frac{1}{L} = \sum_{i=0}^{i=n-1} \frac{1}{L_i} = \sum_{i=0}^{i=n-1} \left[\frac{1}{L_1 \left(1 - \frac{i}{n}\right)} \right] , \tag{12}$$

$$\frac{L_1}{L} = \sum_{i=0}^{i=n-1} \left(\frac{1}{1 - \frac{i}{n}} \right) , \tag{13}$$

or

$$\frac{L_1}{L} = 1 + \sum_{i=1}^{i=n-1} \left(\frac{1}{1 - \frac{i}{n}} \right) \tag{14}$$

It is assumed that there is no current flowing into the last element of the compressor coil, eliminating the infinite term for $i = n$ This is equivalent to a residual inductance at the end of the compressor coil representing the inductance of the backstrap lead to the annular electrode Since

$$0 < 1 - \frac{1}{n} < 1 \quad , \qquad \text{then} \qquad \frac{L_1}{L} > 1$$

The initial inductance L_1 will be larger than the effective inductance The plasma flow into the compressor coil will, therefore, reduce the inductance in the equivalent circuit from the initial value L_1 to the value L

In the increasing inductance mode, the compressor coil is connected directly to the annular electrode Then the inductance in the equivalent circuit will increase as the plasma moves into the compressor coil.

Both configurations were tried The decreasing inductance configuration was selected for further investigation after initial experiments indicated that it would be more efficient for the acceleration of glass beads with diameters between 100 and 700 microns These were attached to a Mylar foil and then placed across the hole in the coil space plate

IV. THEORETICAL INVESTIGATION

Artsimovitch [8] developed the theory of the rail-type accelerator Other investigators have extended this theory to describe the coaxial accelerator The coaxial accelerator with a compressor coil can be represented by an equivalent circuit which consists of the coaxial accelerator circuit to which is added a mesh with variable plasma resistance and a variable inductance simulating the compressor coil An additional switch is incorporated in the mesh to simulate the arrival of the plasma in the coil

A. The Equivalent Circuit

In Figure 11 the acceleration of the plasma in the coaxial accelerator is represented by the variable inductance L_2 L_0 and R_2 are the capacitor bank inductance and resistance, which are constants The resistance R_1 simulates the arrival of the plasma at the compressor coil and L_1 simulates the compressor coil inductance (see previous discussion of compressor coil configuration). The differential equations for this equivalent circuit with the additional switch closed are

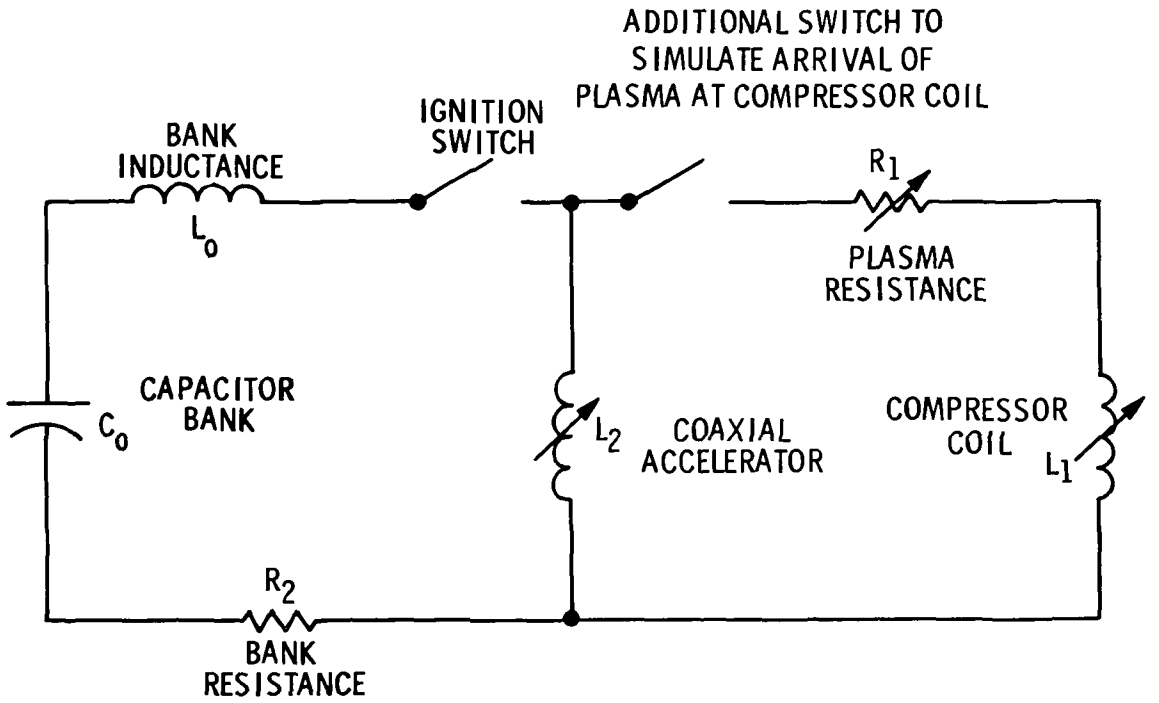

Figure 11 Equivalent circuit for coaxial accelerator with compressor coil

$$U_0 - \frac{1}{C_0} \int_0^t (I1 + I2)\, dt = L_0 \frac{d}{dt} (I1 + I2) + R2\,(I1 + I2) + R1\, I1$$

$$+ \frac{d}{dt} (L1\, I1) \qquad (15)$$

and

$$U_0 - \frac{1}{C_0} \int_0^t (I1 + I2)\, dt = L_0 \frac{d}{dt} (I1 + I2) + R2\,(I1 + I2) + \frac{d}{dt} (L2\, I2) \qquad (16)$$

I1 is the current in the compressor coil and I2 is the current in the coaxial accelerator.

A nondimensional notation is now introduced. With

$$\omega_0^2 = \frac{1}{L_0 C_0} \quad , \tag{17}$$

the time becomes

$$t = \frac{T}{\omega_0} \quad , \tag{18}$$

and the time derivatives are

$$\frac{d}{dt} = \omega_0 \frac{d}{dT} \tag{19}$$

and

$$\frac{d^2}{dt^2} = \omega_0^2 \frac{d^2}{dT^2} \tag{20}$$

The nondimensional currents are

$$X1, X2 = \frac{I1, 2}{\omega_0 U_0 C_0} \quad , \tag{21}$$

the nondimensional inductances are

$$X3, X4 = \frac{L1, 2}{L_0} \quad , \tag{22}$$

and the nondimensional resistance terms are

$$X5, X6 = \frac{R1, 2}{\omega_0 L_0} \tag{23}$$

Then the differential equations (15) and (16) may be written

$$1 - \int_0^T (X1 + X2)\, dT = \frac{d}{dT}(X1 + X2) + X6\,(X1 + X2) + X5\, X1 + \frac{d}{dT}(X1\, X3) \tag{24}$$

and

$$1 - \int_0^T (X1 + X2)\, dT = \frac{d}{dT}(X1 + X2) + X6\,(X1 + X2) + \frac{d}{dT}(X2\, X4) \tag{25}$$

The initial values at $T = 0$ are

$$X1 = 0 \tag{26}$$

and

$$X2 = 0 \tag{27}$$

With these values, the first derivatives are determined from equations (24) and (25),

$$\left(\frac{dX1}{dT}\right)_{T=0} = \frac{X4}{X3 + X4 + X3\, X4} \tag{28}$$

and

$$\left(\frac{dX2}{dT}\right)_{T=0} = \frac{X3}{X3 + X4 + X3\ X4} \qquad (29)$$

The differential equations (24) and (25) are then differentiated to eliminate the integrals

$$-(X1 + X2) = \frac{d^2}{dT^2}(X1 + X2) + X6\frac{d}{dT}(X1 + X2) + \frac{d}{dT}(X5\ X1) + \frac{d^2}{dT^2}(X3\ X1) \qquad (30)$$

and

$$-(X1 + X2) = \frac{d^2}{dT^2}(X1 + X2) + X6\frac{d}{dT}(X1 + X2) + \frac{d^2}{dT^2}(X2\ X4) \qquad (31)$$

In these equations X6 is a constant.

B. Analytical Solution for a Simplified Case

Equation (31) is subtracted from equation (30)

$$\frac{d^2}{dT^2}(X1\ X3 - X2\ X4) + \frac{d}{dT}(X1\ X5) = 0 \qquad (32)$$

The result of the first integration is

$$\frac{d}{dT}(X1\ X3 - X2\ X4) + X1\ X5 = C \qquad (33)$$

Using the initial values from equations (26), (27), (28), and (29),

$$C = X3\frac{dX1}{dT} - X4\frac{dX2}{dT} = 0 \qquad (34)$$

Equation (33) then becomes a first order differential equation for X1 if the other functions X are known,

$$\frac{dX1}{dT} + X1 \left[\frac{d\,(\ln X3)}{dT} + \frac{X5}{X3} \right] - \frac{1}{X3} \frac{d}{dT} (X2\ X4) = 0 \qquad (35)$$

The experimental results indicate that during the first half-period of the discharge the current through the coaxial accelerator, X2, may be approximated by the undamped capacitor bank current with a frequency

$$\omega_0 = \frac{1}{\sqrt{L_0\ C_0}} \quad , \qquad (36)$$

and the maximum current at $T = \pi/2$ becomes

$$I20 = \frac{U_0}{\omega_0\ L_0} \quad , \qquad \text{or} \qquad X20 = 1 \qquad (37)$$

Then,

$$X2 = X20 \sin T = \sin T \qquad (38)$$

This result implies that the inductance of the coaxial accelerator does not change, X4 = X40 = constant Other approximations are necessary for the functions X3 and X5 The decrease of the compressor coil inductance is represented arbitrarily as

$$X3 = \frac{X30}{(1 + T)^m} \quad , \quad \text{where} \quad X30 = X3 \text{ at } T = 0 \quad , \qquad (39)$$

and the arrival of the plasma at the compressor coil is approximated by

$$X5 = \frac{X50}{(1 + T)^n} \quad , \qquad \text{where} \qquad X50 = X5 \text{ at } T = 0 \qquad (40)$$

Then the differential equation (35) for X1 becomes

$$\frac{dX1}{dT} + X1 \left[\frac{d(\ln X3)}{dT} + \frac{X50}{X30} (1 + T)^{n-m} \right] - \frac{X40}{X30} (1 + T)^{m} \cos T = 0 \quad . \tag{41}$$

For n = m, the solution for X1 is

$$X1 = \frac{X40}{X30} \left[\frac{(1 + T)^{n}}{\left(\frac{X50}{X30}\right)^{2} + 1} \right] \left[\frac{X50}{X30} \sin T + \exp \left(- \frac{X50}{X30} T \right) - \cos T \right] , \tag{42}$$

and if the parameters

$$\frac{X40}{X30} = \frac{L20}{L10} \tag{43}$$

and

$$\frac{X50}{X30} = \frac{R10}{\omega_0 L10} \tag{44}$$

are set equal to 1, a very simple expression is obtained,

$$X1 = \frac{(1 + T)^{n}}{2} \left[\sin T - \cos T + \exp (- T) \right] \tag{45}$$

The nondimensional functions X1 and X2 for the currents are plotted in Figure 12 for various values of equations (43), (44), and n = 0.5

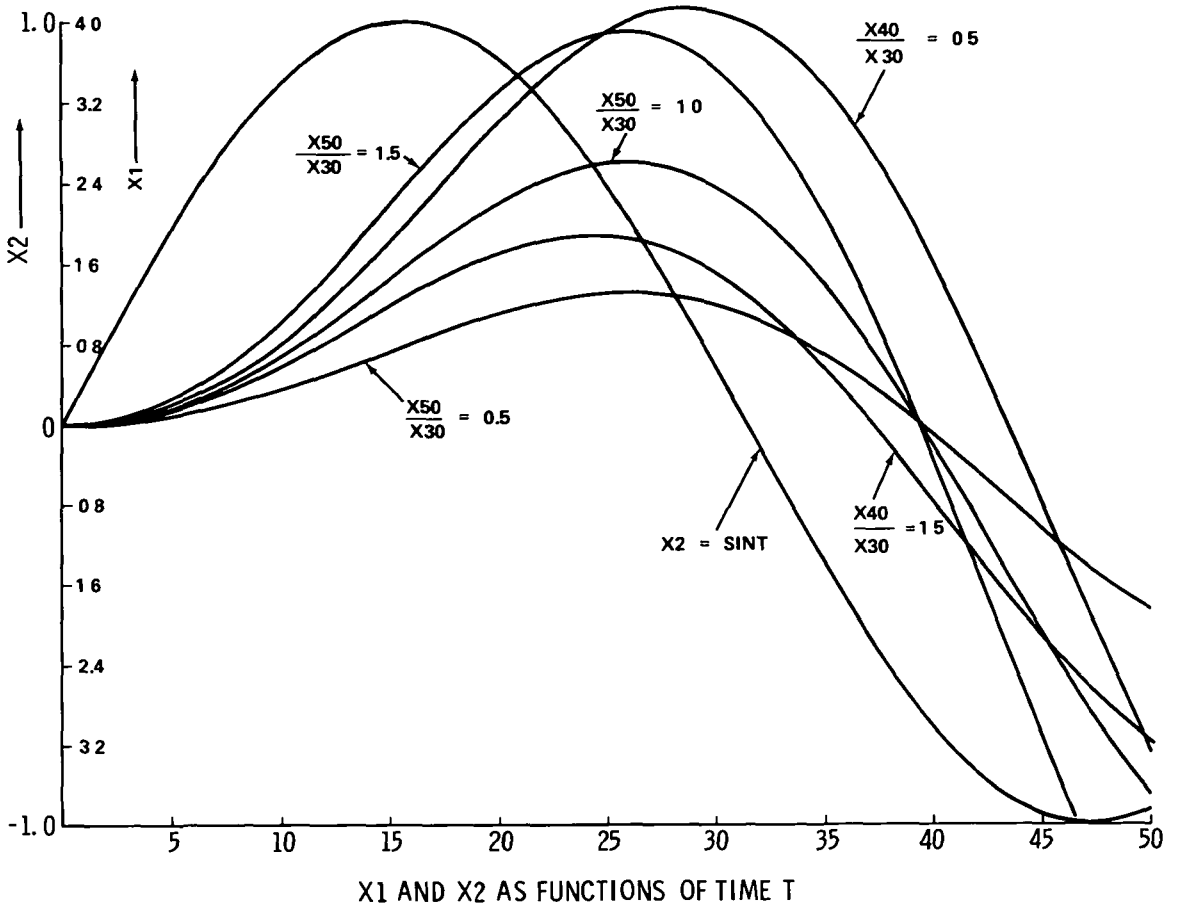

Figure 12. Compressor coil current from equation (44)

C. Numerical Integration of the Equations for the Equivalent Circuit

For the numerical integration the differential equations (32) and (33) are rewritten

$$\frac{d^2X1}{dT^2} = \left\{ - \left[1 + X4\right]\left[\frac{dX1}{dT}\left(X6 + X5 + 2\frac{dX3}{dT}\right) + X6\frac{dX2}{dT} + X1\left(1 + \frac{dX5}{dT} + \frac{d^2X3}{dT^2}\right) + X2\right]\right.$$

$$\left. + X6\frac{dX1}{dT} + \left(X6 + 2\frac{dX4}{dT}\right)\frac{dX2}{dT} + X1 + X2\left(1 + \frac{d^2X4}{dT^2}\right)\right\} \Bigg/ \left[(1 + X3)(1 + X4) - 1\right] \tag{46}$$

and

$$\frac{d^2X2}{dT^2} = \left\{ - \left[1 + X3\right] \left[X6 \frac{dX1}{dT} + \left(X6 + \frac{2dX4}{dT}\right) \frac{dX2}{dT} + X1 + X2 \left(1 + \frac{d^2X4}{dT^2}\right)\right] \right.$$

$$+ \frac{dX1}{dT} \left(X5 + X6 + 2 \frac{dX3}{dT}\right) + X6 \frac{dX2}{dT} + X1 \left(1 + \frac{dX5}{dT} + \frac{d^2X3}{dT^2}\right)$$

$$\left. + X2 \right\} \Big/ \left[(1 + X3)(1 + X4) - 1\right] \qquad (47)$$

Equations (46) and (47) are integrated in four sequential steps The motion of the plasma in the coaxial accelerator is described during the first step The second step begins when the plasma enters the compressor coil and ends when the plasma reaches the downstream (narrow) end of the compressor coil The next step describes the behavior of the system during the remaining part of the compression phase which ends at the compressor coil current maximum During the fourth step the compressor coil current will decrease

1 Calculation of Step 1 During the first phase of the discharge, when the plasma is still inside the coaxial accelerator, there will be no electrical current in the compressor coil. To simulate this condition a switch is added to the compressor coil loop of the equivalent circuit shown in Figure 11 This switch is open as long as the plasma is in the coaxial accelerator Step 1 is, therefore, described by the differential equation for the coaxial accelerator current which is obtained from equation (33) with X1 and dX1/dT set equal 0,

$$\frac{d^2X2}{dT^2} = \left[- X2 \left(1 + \frac{d^2X4}{dT^2}\right) - \frac{dX2}{dT} \left(X6 + 2 \frac{dX4}{dT}\right)\right] \Big/ (1 + X4) \qquad (48)$$

The coaxial accelerator inductance X4 changes with the position of the plasma during the acceleration process. The force F_z acting upon the plasma, which is assumed to be a mass m at the position z of the coaxial accelerator, can be determined from the partial derivative of the energy W of the configuration with respect to the coordinate in which the plasma motion is directed,

$$F_z = \frac{\partial W}{\partial z} = \frac{\partial}{\partial z} \left(L2 \frac{(I2)^2}{2}\right) \qquad (49)$$

The inductance representing the coaxial accelerator in the equivalent circuit changes with the plasma position Z in the coaxial accelerator,

$$L2 = L20 + bz \quad , \tag{50}$$

where

$$L20 = L2 \quad \text{at} \quad T = 0 \quad , \quad z = 0 \quad , \tag{51}$$

and b is the gradient of the inductance of the coaxial accelerator

$$b = \frac{\mu_0}{2\pi} \ln a \quad , \tag{52}$$

where

$$a = \frac{\text{radius of outer electrode}}{\text{radius of inner electrode}} \tag{53}$$

The force F_Z acting upon the plasma mass m is then

$$F_Z = m \frac{d^2 Z}{d t^2} = \frac{I^2 b}{2} \quad . \tag{54}$$

With the nondimensional coordinate

$$X7 = \frac{b}{L_0} Z \tag{55}$$

and the constant

$$K7 = \frac{b^2 C_0^2 U_0^2}{2m L_0} \quad , \tag{56}$$

the equation of motion for the plasma is

$$\frac{d^2 X7}{dT^2} = k7\ (X2)^2 \tag{57}$$

The inductance X4 is determined from equation (50) which is divided by L_0 for nondimensional notation,

$$X4 = X40 + X7 \quad , \tag{58}$$

with X40 equal to the nondimensional inductance of the coaxial accelerator at T = 0 and X7 is calculated by integrating equations (57) and (58) The initial values for these equations at T = 0 are X2 = 0, and

$$\frac{dX2}{dT} = \frac{1}{1 + X4} \tag{59}$$

The plasma motion starts at z = 0, with the velocity 0, therefore,

$$X7 = 0 \quad , \tag{60}$$

and

$$\frac{dX7}{dT} = 0 \tag{61}$$

Using these initial values, the differential equations (48) and (57) are integrated until the nondimensional coordinate X7 reaches the value attained at the end of the coaxial accelerator, X7 = X71.

2. Calculation of Step 2 At the beginning of Step 2 the switch in the compressor coil loop is closed as the plasma moves into the compressor coil In a first approximation (see previous discussion of compressor coil configuration), the plasma velocity is set constant and equal to the value at the end of step 1

$$\frac{dX7}{dT} = \left(\frac{dX7}{dT}\right)_{X7 = X71} \quad . \tag{62}$$

The time needed for the plasma to reach the downstream (narrow) end of the compressor coil with the coordinate X72 is then

$$T2 = \frac{X72}{\left(\frac{dX7}{dT}\right)_{X7 = X71}} \tag{63}$$

During Step 2, the compressor coil inductance decreases from the initial value X31 to a lower value if the configuration operates in the decreasing inductance mode. This behavior is approximated by a linear function of the time T,

$$X3 = X31 \left(1 - K1 \frac{T - T1}{T2 - T1}\right) \quad , \tag{64}$$

where

$$X31 = X3 \quad \text{at} \quad T = T1 \quad ,$$

and where a free constant K1 can be used to adjust the theoretical results to fit the experiment Another linear function of T and a free constant K2 is used to simulate the decreasing resistance between the center electrode and the compressor coil which drops from a high initial value X51 to the plasma resistance

$$X5 = X51 \left(1 - K2 \frac{T - T1}{T2 - T1}\right) \quad , \tag{65}$$

where

$$X51 = X5 \quad \text{at} \quad T = T1$$

It is assumed that the inductance of the coaxial accelerator does not change after the plasma has reached the end of the accelerator at step 1, X4 = X41. The initial values for the electrical currents are

$$X1 = 0 \quad \text{and} \quad X2 \text{ is equal to the final value of step 1} \tag{66}$$

The first derivatives are determined from equations (24) and (28) at T = T1 Equation (28) can be rewritten as

$$\frac{dX1}{dT} = \frac{X4}{X3}\frac{dX2}{dT} \quad , \tag{67}$$

and equation (24) at T = T1 is

$$1 - \int_{T=0}^{T=T1} X2dT = \frac{d}{dT}(X1 + X2) + X2\,X6 + \frac{d}{dT}(X1\,X3) \quad . \tag{68}$$

Using equation (67), the first derivative of X2 is obtained

$$\frac{dX2}{dT} = \frac{1 - \int_{T=0}^{T=T1} X2dT - X2\,X6}{1 + X4\left(1 + \frac{1}{X3}\right)} \quad , \tag{69}$$

and the first derivative of X1 is

$$\frac{dX1}{dT} = \frac{X4}{X3}\left[\frac{1 - \int_{T=0}^{T=T1} X2dT - X2\,X6}{1 + X4\left(1 + \frac{1}{X3}\right)}\right] \tag{70}$$

The integral

$$\int_{T=0}^{T=T1} X2\, dT \tag{71}$$

is evaluated during Step 1. Using these initial values, the differential equations (46) and (47) are integrated until T = T2

3 Calculation of Step 3 During Step 3 the inductance X3 and the resistance X5 remain constant and have the same value as at the end of Step 2. The compressor coil current X1 and the coaxial accelerator current X2 have initial values which are equal to the final values of Step 2 The initial values for the first derivatives of the current functions are calculated using equations (24) and (25), which are solved for dX1/dT and dX2/dT

$$\frac{dX1}{dT} = \frac{X4\,[1 - X11 - X6\,(X1 + X2) - (1 + X4)\,X1\,X5]}{X3 + X4 + X3\,X4} \tag{72}$$

and

$$\frac{dX2}{dT} = \frac{X3\,[1 - X11 - X6\,(X1 + X2)] + X1\,X5}{X3 + X4 + X3\,X4}\,, \tag{73}$$

where $X11 = \int_0^T (X1 + X2)dT$

Equations (46) and (47) may now be integrated until the compressor coil current X1 has reached its maximum.

4 Calculation of Step 4. Again it is assumed that X3 and X5 do not change with time The initial values are obtained in the same way as in Step 3 During this step there will be a decompression The integration is terminated after a time corresponding to the time recorded on the oscilloscope during the discharge, usually 100 microseconds. The computations have been performed at the Leibniz Rechenzentrum of the Bayerische Akademie der Wissenschaften at the Technische Universität München, Germany.

V. EXPERIMENTAL AND THEORETICAL RESULTS

The theory developed in the preceding section is compared with experiments performed in the Plasma Hypervelocity Range of the Space Sciences Laboratory at the George C. Marshall Space Flight Center

A. Plasma Flow

The theory can be correlated with a specific experiment through the elements of the equivalent circuit shown in Figure 11 The inductance of the compressor coil L_1 and the inductance of the capacitor bank with coaxial cables and switch assembly L_0 were measured prior to the experiment [11] Throughout the experiments described here, the capacitor bank and the switch assembly have not been changed. Then the only unknown quantities are the plasma resistance R_1 and the constants K1, K2, and K7

The plasma resistance has little influence upon the characteristics of the equivalent circuit. It may be regarded as part of the impedance Z of the circuit mesh with compressor coil inductance L_1, where

$$z = \sqrt{R_1^2 + \omega^2 L_1^2} \tag{74}$$

A typical example is

$$R1 = 4.8 \times 10^{-3} \text{ ohm} \tag{75}$$

and

$$L1 = 2 \times 10^{-6} \text{ hy}$$

from the experiment described in Table 2 The frequency is

$$\omega = 9.45 \times 10^{4} \text{ sec}^{-1} \tag{76}$$

Then the plasma resistance term is three orders of magnitude smaller than the inductance term.

The increase of the coaxial accelerator inductance L_2 in Step 1 is proportional to the constant K7 Equation (58) may be rewritten as

$$K7 = \frac{U_0^2 C_0}{2m} \frac{b^2 C_0}{L_0} \quad . \tag{77}$$

The first term of equation (77) is the stored energy per plasma mass m For a coaxial accelerator with given geometry and constant plasma mass, K7 changes with the capacitor bank charging voltage U_0 The results of the computation of the plasma velocity at the end of a coaxial accelerator 14 cm long are compared with measured values in Figure 13 For this example, K7 = 1 0 corresponds to a charging voltage of 18 kV The plasma velocity was measured with two light probes located 20 cm apart, one at the end of the coaxial accelerator and the other behind the compressor coil The order of magnitude of the velocity from theory and experiment is the same The velocity increases with larger values of U_0 The light probes could only measure the propagation velocity of a luminous front, which may not coincide with the major portion of the plasma mass.

The photographic recording of the oscilloscope trace of the current in the compressor coil as well as the capacitor bank voltage indicates the time when the plasma left the coaxial accelerator The capacitor bank voltage recordings show irregularity when the compressor coil current begins to rise The arrival time has been plotted in Figure 14 as a function of the capacitor bank charging voltage U_0 For comparison, the recordings of the first light detector used for velocity measurement are also shown. The third curve in this figure represents the values calculated using the first step outlined in the previous section, equations (57) and (48). The experimental data are listed in Table 3

1 Capacitor Bank Voltage The capacitor bank voltage measurement was described in the section on diagnostics and particle velocity measurement. The voltage across the capacitor bank is

$$\frac{U}{U_0} = 1 - \int_0^T (X1 + X2)\, dT \tag{78}$$

(see equations (24) and (25))

The recorded curve is compared with the calculated curve in Figure 15 The experimental curve shows a potential drop approximately 30 microseconds after initiation of the discharge This potential drop has also been observed without the compressor coil, and it coincides approximately with the transition of the coaxial accelerator current

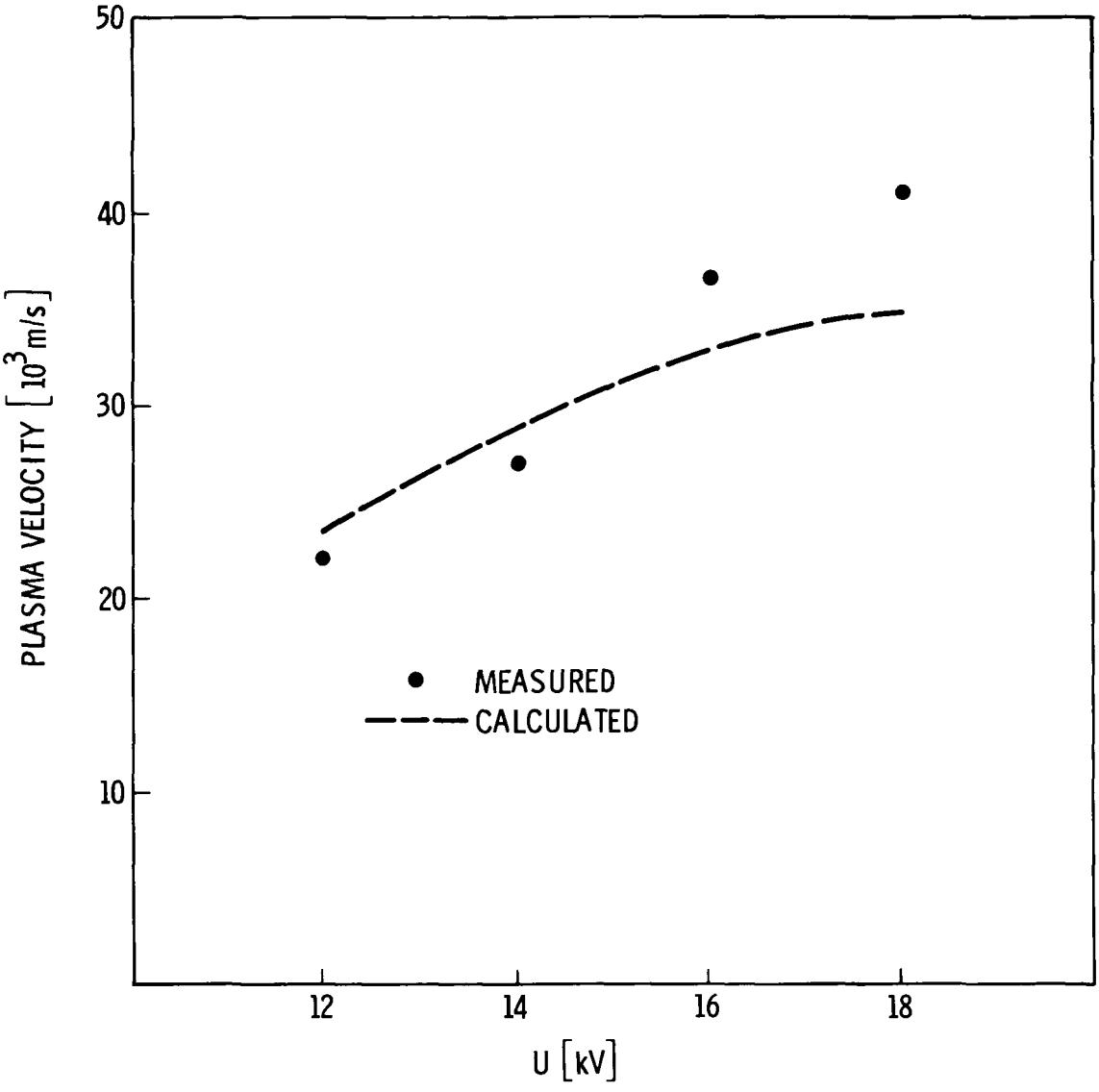

Figure 13 Plasma velocity at the end of the coaxial accelerator.

through zero. If the coaxial accelerator is still filled with a plasma, then another discharge can be initiated, causing a shift in the potential drop There is an indication of the same effect after another half-period of the discharge During these experiments with different compressor coil configurations, high-speed motion pictures were tried. A camera with up to 20,000 frames per second was used so that the exposure time corresponded roughly to one half-period of the discharge. These motion pictures did not give detailed information

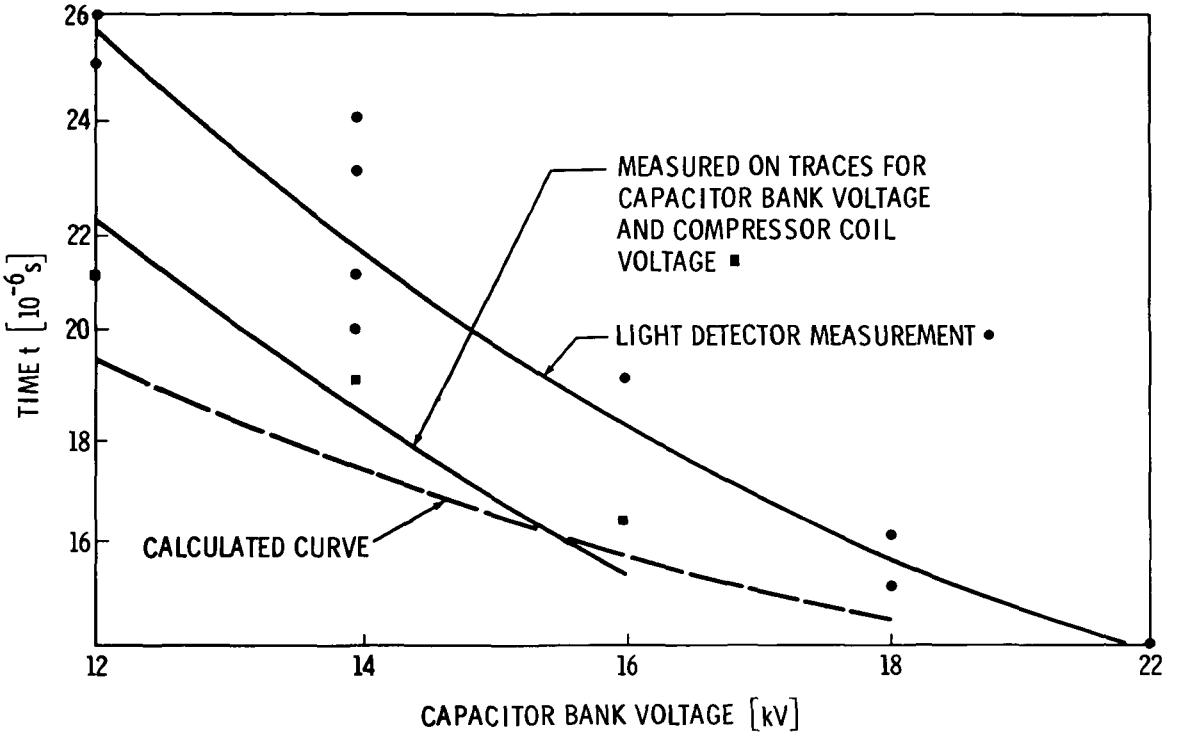

Figure 14 Time of arrival of the plasma at the compressor coil.

about the compressor coil flow, but they showed that there were several subsequent accelerations of plasma clouds These observations tend to confirm the explanation given for the potential drop observed on the experimental curve The measured frequency of the discharge was nearly constant during the experiments, varying only by 2 microseconds The integrations of the equivalent circuit equations with different values for the compressor coil inductance showed the same behavior The frequency of the discharge is, therefore, mainly determined by the capacitor bank values C_0 and L_0.

2. Compressor Coil Current. The magnitude and the change with time of the compressor coil current determine the efficiency of the compressor coil. The experimental curve is compared with the calculated curve in Figure 16 During these experiments, the amplitude of the compressor coil current trace was not calibrated. The absolute value of the compressor coil current can, therefore, only be estimated from the comparison with the theory The theory shows that the magnitude of the compressor coil current depends upon the ratio of the inductances L_0, L_1, and L_2, all of which are well known It, therefore, seems justifiable to use the correlation between theory and experiment to estimate the magnitude of the compressor coil current Rewriting equation (30),

$$I1 = X1\ \omega_0\ U_0\ C_0$$

TABLE 3 EXPERIMENTAL AND THEORETICAL DATA

Data describing the experiment	
Bank capacitance	$C_0 = 2.7 \times 10^{-4}$ F
Bank inductance	$L_0 = 4.16 \times 10^{-7}$ Hy
Bank resistance	$R_2 = 7\,9 \times 10^{-3}$ Ohm
Coaxial accelerator inductance	$L_2 = 0.72 \times 10^{-6}$ Hy
Compressor coil inductance	$L_1 = 4\,43 \times 10^{-7}$ Hy
Coaxial accelerator inductance per unit length	$b = 3.58 \times 10^{-7}$ Hy/m
Coaxial accelerator length (for plasma acceleration)	20 cm
Compressor coil length	13 cm
Plasma resistance	$R_1 = 4\,8 \times 10^{-3}$ Ohm
Aluminum foil mass	m = 0.04 g
Glass particle diameter	D = 0 25 mm
Charging voltage	U_0 = 16 kV
Measured particle velocity	v = 5 3 km/s

Data used for the theory	
X30 = 0.4	K2 = 0 999
X40 = 0 173	K4 = 0.324
X50 = 1 8	K5 = 0.204
X6 = 0 2	K7 = 0 7
K1 = 0 5	

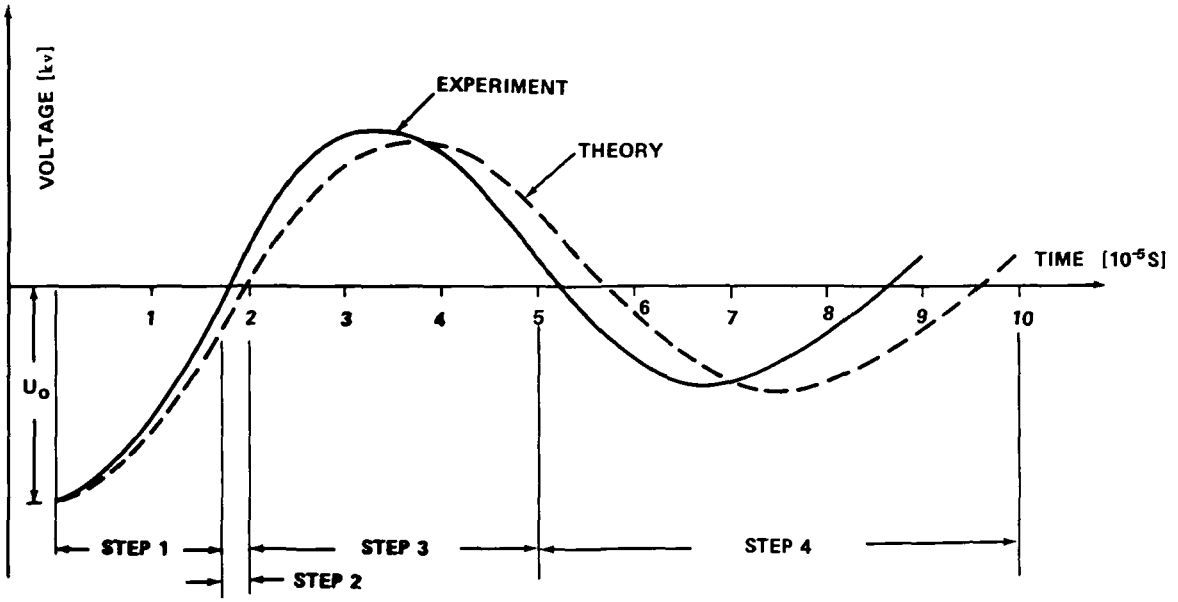

CAPACITOR BANK VOLTAGE AS A FUNCTION OF TIME FOR K7 = 0.7

Figure 15 Capacitor bank voltage

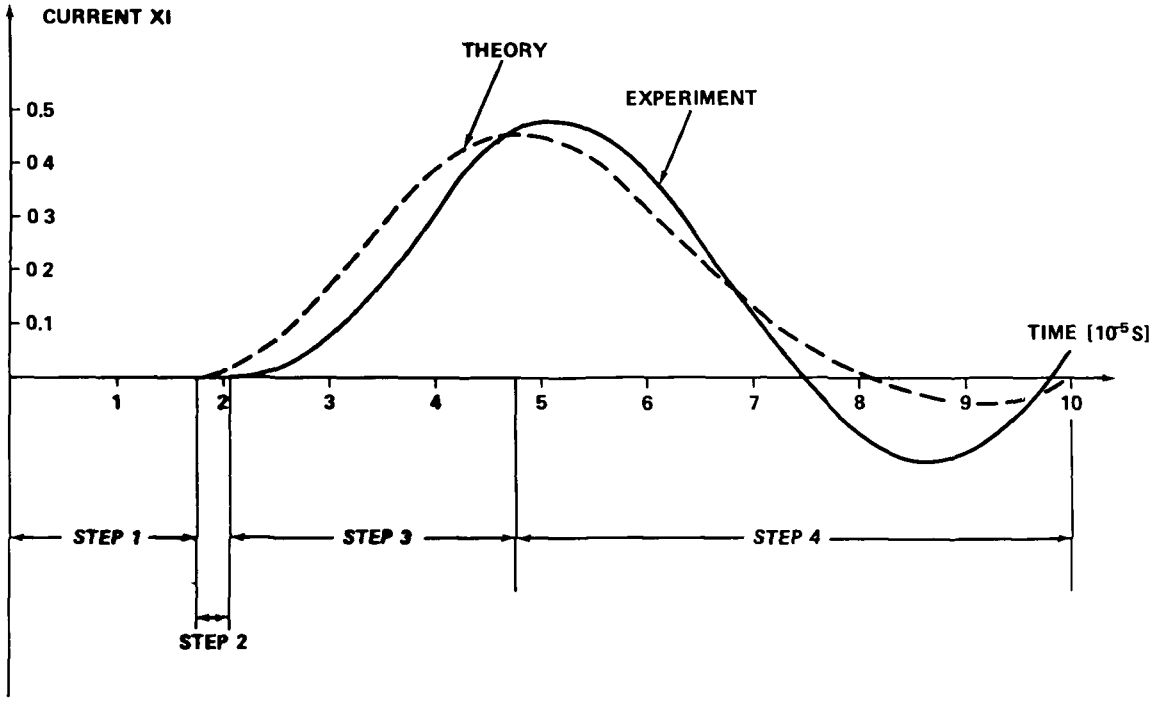

COMPRESSOR COIL CURRENT AS FUNCTION OF TIME FOR K7 =0.7

Figure 16. Compressor coil current

With the values given in Table 3, the maximum value of the compressor coil current becomes

$$I1_{max} = 4\,08 \times 10^5 \times 1 = 4\,96 \times 10^4 \text{ A} \tag{79}$$

The magnetogasdynamic flow in the vicinity of the compressor coil axis can be described by the nonviscous magnetogasdynamic momentum equation,

$$\rho \frac{d\,\bar{v}}{d\,t} = - \text{grad } p + \bar{j} \times \bar{B} \tag{80}$$

The magnetogasdynamic force arises from the interaction of the electric current density

$$\bar{j} = \sigma (\bar{E} + \bar{v} \times \bar{B}) \quad , \tag{81}$$

with the magnetic induction $\bar{B}$.

$$\bar{B} = \mu \bar{H} \tag{82}$$

The components of the vector product $\bar{j} \times \bar{B}$ are, in cylindrical coordinates,

$$\bar{j} \times \bar{B} = \begin{pmatrix} j_\phi B_z - j_z B_\phi \\ j_z B_r - j_r B_z \\ j_r B_\phi - j_\phi B_r \end{pmatrix} \tag{83}$$

The radial component will perform the compression of the plasma The current density j_ϕ is

$$j_\phi = \sigma (E_\phi + v_z B_r) \tag{84}$$

The first term in equation (84) comes from the change of the magnetic field with time,

$$\dot{\overline{H}} = - \frac{1}{\mu} \overline{\nabla} \times \overline{E} \quad . \tag{85}$$

The axial field on the compressor coil axis can be written

$$H_z \approx A(z)\, I(t) \quad , \tag{86}$$

where A(z) is a function derived from the compressor coil geometry and I(t) is the compressor coil current. By integrating equation (85), the azimuthal electrical field from the time varying magnetic field becomes

$$E_\phi \approx - \frac{r}{2} \mu\, A(z)\, I(t) \tag{87}$$

The second term of equation (84) is the product of the axial plasma velocity and the radial magnetic field. The latter can be approximated with the assumption that the axial magnetic field does not change in the vicinity of the compressor coil axis with the radius r. Then

$$\overline{\nabla} \quad \overline{H} = 0 \tag{88}$$

gives an approximation for the radial magnetic field,

$$H_r \approx - \frac{r}{2} \frac{d\, A(z)}{d\, z} I(t) \tag{89}$$

The azimuthal electrical current density is then

$$J_\phi = - \frac{\sigma\, \mu}{2} r \left[A(z) \frac{d\, I(t)}{dt} + v_z \frac{d\, A(z)}{dz} I(t) \right] \tag{90}$$

The first term of the radial force acting upon the plasma is the product of this current density with the axial magnetic inductance,

$$F_r = j_\phi B_r = \frac{\sigma \mu^2}{2} r A(z) I(t) \left[A(z) \frac{dI(t)}{dt} + v_z \frac{d A(z)}{dz} I(t) \right] \quad (91)$$

As long as F_r is negative, the force acts towards the axis and the plasma is compressed in the coil. The first term is negative during the first quarter period of the compressor coil current when the time derivative of the magnetic induction is positive The sign of the second term depends upon the direction of the radial magnetic field This will be negative approximately the first 80 percent of the coil length The second term in the radial component of the magnetogasdynamic force, equation (83), will always be negative It is the interaction between the axial current density from the center electrode to the compressor coil with the azimuthal magnetic field induced by this current density.

The azimuthal component of the magnetogasdynamic force produces an azimuthal plasma velocity which is small near the compressor coil axis because of the symmetry of the configuration. The axial component of the force F_z may not be negative if there is to be particle acceleration. The square of the flow velocity in equation (1) indicates that the axial term,

$$F_z = j_r B_\phi - j_\phi B_r \quad , \quad (92)$$

should always be positive A first approximation would be that these forces are transferred without delay into thermodynamic quantities such as pressure and density. The compressor coil, therefore, increases the density of the plasma flow leaving the coaxial accelerator. The experiment shows that the compression is terminated when the compressor coil current is at its maximum value.

The comparison of theory and experiment shows that the equivalent circuit and the corresponding theory described in the foregoing section simulate the characteristics of the coaxial accelerator with attached compressor coil One of the principal reasons is that the behavior of the experiment, as well as the equivalent circuit used for the theory, is dominated by the capacitance C_0 and the inductance L_0 of the capacitor bank, coaxial cables, and switch assembly, and the ratio of L_0 to the inductances of the coaxial accelerator L_2 and the compressor coil L_1.

3. Coaxial Accelerator Current The voltage measured at the capacitor bank switch assembly can be differentiated to obtain the total current flow, $I_1 + I_2$, to the coaxial accelerator and compressor coil There was no separate measurement of the coaxial accelerator current during the experiments described here because the compressor coil was grounded to the coaxial accelerator outer electrode (Fig 3).

The theoretical curves for X2 and X1 + X2 have been calculated using the theory which has been previously shown to agree with the experimental curves of Figures 15 and 16. They are shown in Figure 17. The third curve shows the current in an equivalent circuit, which contains only the capacitor bank elements and the coaxial accelerator The three curves are identical during Step 1 of the first and second curves. The third curve is obtained by extending the integration of Step 1 until T = 10.0

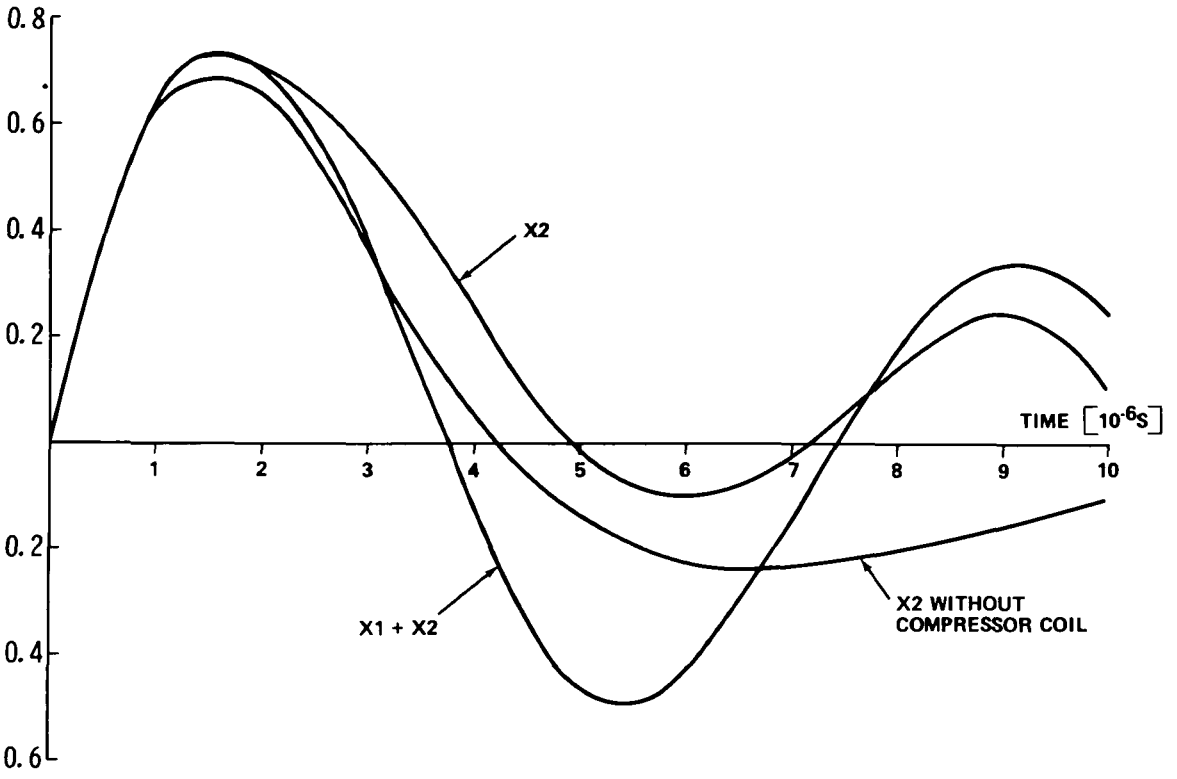

CURRENT (X1 + X2) AND X2 AS A FUNCTION OF TIME FOR K7 = 0.7

Figure 17. Coaxial accelerator current

B. Particle Acceleration

The acceleration of the particles placed on a Mylar foil across the narrow end of the compressor coil can be used as an indication of the amount of compression of the discharge. Figure 18 is a photograph of the beads after they have left the Mylar foil They have an initial diameter of 0 8 mm and a velocity of 4 to 5 km/s The velocity measurement method has been described previously During the experiments the pressure in the range was always kept below 25 microns, and the capacitor bank charging voltage and the particle initial diameter were varied. Only spherical glass beads were used

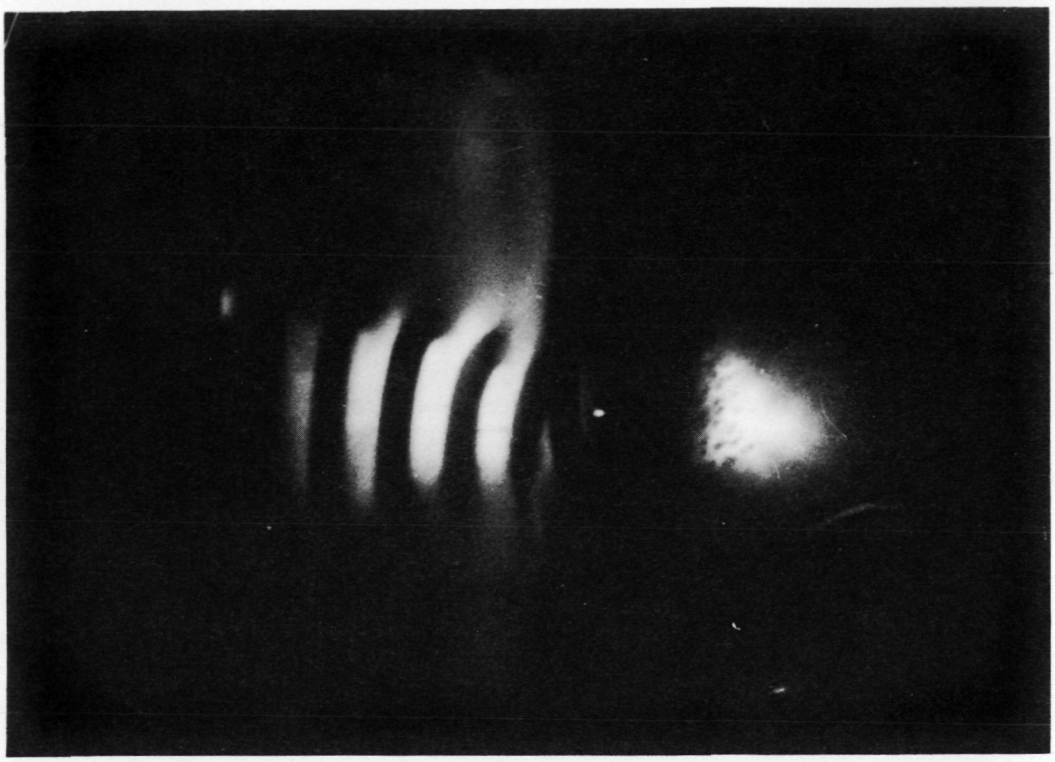

Figure 18. Photograph of accelerated particles in compressor coil plasma flow.

Figure 19 shows the particle velocity as a function of the capacitor bank charging voltage for three initial particle diameters. The dashed curve in these figures is obtained from the assumption that after the acceleration, kinetic energy of the particles with the mass m_p is proportional to the energy stored in the capacitor bank, $C_0 U_0{}^2/2$, multiplied by the particle cross section S and a coefficient C_1 representing the energy transfer efficiency

$$\frac{m_p}{2} v^2 = C_1 S \frac{C_0^2 U_0^2}{2} \quad . \tag{93}$$

Then the velocity of a particle with the initial diameter D is given by

$$v = C_2 \frac{U_0}{\sqrt{D}} \quad , \quad \text{where} \quad C_2 = \sqrt{\frac{3 C_1 C_0}{2 \rho_{GLASS}}} \quad . \tag{94}$$

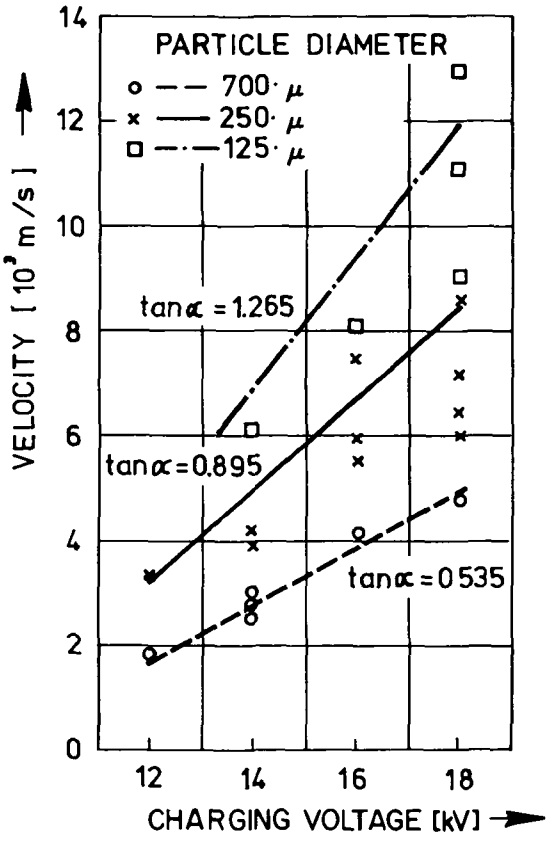

Figure 19 Particle velocity as function of capacitor bank charging voltage.

In the case of the 700-micron diameter particle, the straight line representing this theory could easily be drawn through the experimental results The theoretical line for another particle initial diameter will have an inclination which is related to the 700-micron curve inclination by

$$\frac{\tan \alpha}{\tan \alpha_{700}} = \left(\frac{700}{D}\right)^{1/2} \qquad (95)$$

The inclinations of the curves in the figures for the 250-micron and the 125-micron particles were calculated from this formula The absolute level of these curves was adjusted to the 700-micron experiments The constant C_2 in equation (94) was determined from the line approximating the 700-micron results The lines for 250 microns and 125 microns can then be computed with equation (94) In Figure 20 the final velocity is plotted over the particle initial diameter The theoretical curves are also calculated from equation (94)

The difference between the velocities measured in different experiments with the same initial particle size increases with large capacitor bank charging voltage, very probably due to particle ablation during the interaction with the plasma

VI. DESCRIPTION OF THE COMPUTER PROGRAM[1]

The differential equations are integrated numerically in four sequential steps by the SUBROUTINE HPCG The equations for each step are given in the SUBROUTINES FCT1, FCT2, FCT3, and FCT4, which are called by SUBROUTINE HPCG. The output is performed through the SUBROUTINE OUTP

1. A listing of the computer program can be found in the Appendix.

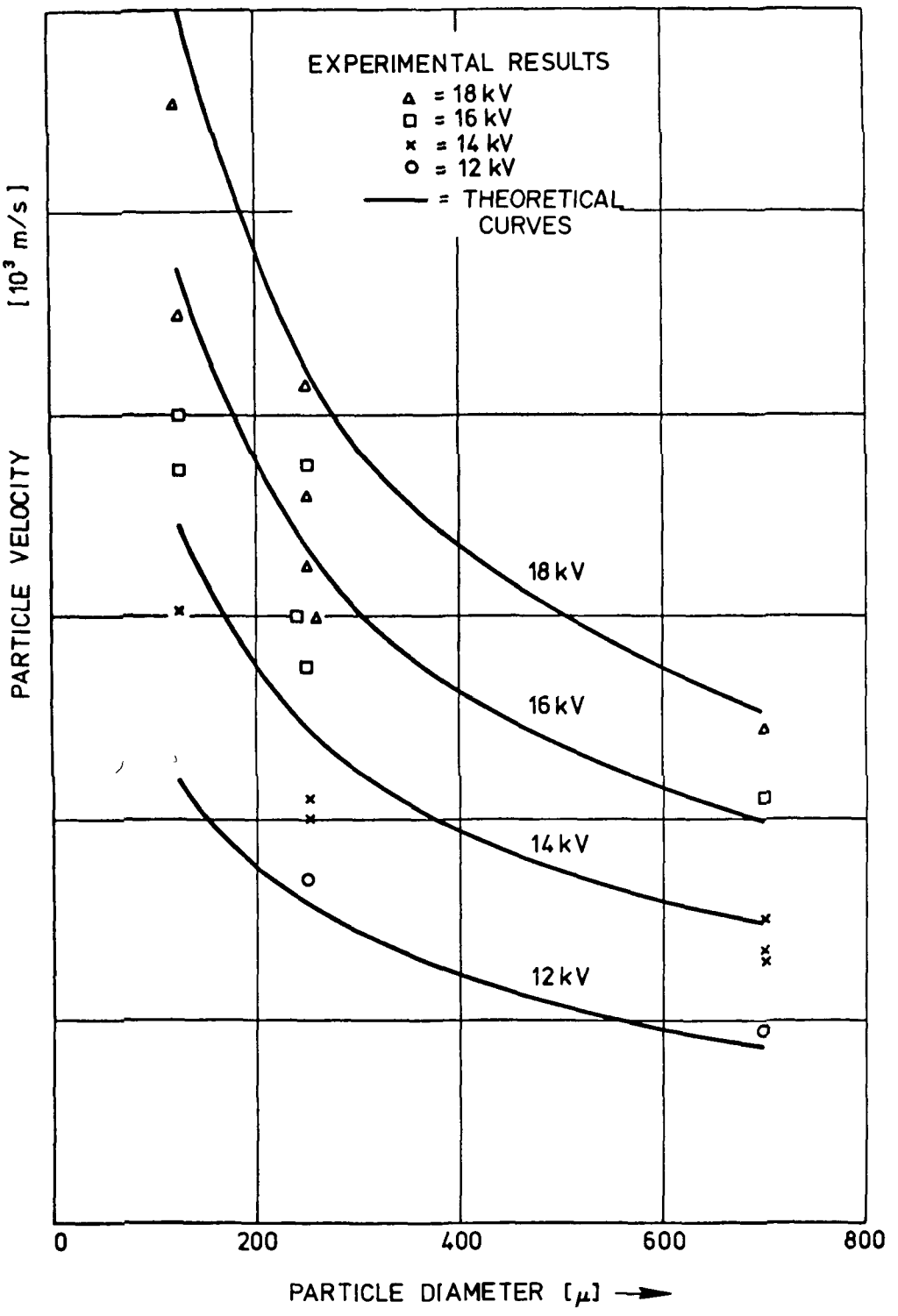

Figure 20 Particle velocity as function of the particle initial diameter

In the program some names are used which are different from those used in the Theoretical Investigation section to avoid changing most of the integration statements in SUBROUTINE HPCG, which was provided by J. Steuerwald[2]. The corresponding names were

Independent variable	T → X
Dependent variable	X1, X2, . X11 → Y(1), . . Y(11)
Constants	K1, K2, .. K7 → VK(1), .. VK(7)

A. Input Data

The input data are given by the MAIN PROGRAM The constants VK(i) and VK(2) were introduced and described in equations (64) and (65), VK(7) in (56), and VK(4) and VK(5) represent the coordinates of the ends of the coaxial accelerator and the compressor coil, respectively. The initial values Y(1) . Y(11) for the computation of starting values for the first integration-step are Y(1), Y(2), Y(7), Y(8), Y(10) and Y(11) are equal to zero at T = 0, Y(3), Y(4) and Y(5), Y(6) represent the nondimensional values for the inductances L1, L2 and the resistances R1, R2. Y(9) is obtained from equation (59) After the output statements for the listing of the input data, several parameters of the integration such as the bounds of the integration interval and the error bound and the initial increment of the independent variable X are furnished to the integration program.

B. Integration

It was not necessary to use different error weights The initial value Y(3) for the coil inductance is stored on "core" for some calculations during STEP 3. If the plotter is on-line, an index (IND) is used to count the calculated elements which are moved to the plotter-storage-array.

With these specifications, SUBROUTINE HPCG begins the integration of the first equation system which is defined in SUBROUTINE FCT1. DERY(1) . DERY(11) are the first derivates of the independent variables DERY(9) is obtained by equations (28) and (29), DERY(10) by (57), and DERY(11) is described in (73) The parameter KKX indicates the number of the integration step, the steps are 1, 2, 3 or 4 and are used by SUBROUTINE OUTP in a control statement for termination HPCG integrates the equations until there is satisfactory accuracy. The calculated values are then transmitted to SUBROUTINE OUTP, where some of them are changed from nondimensional to real values

---

2. J Steuerwald, Instituet fur R. Plasmaphysik, Garching, Germany, private communication

Real Time	RT = X/WO = X 1.06 (10^{-5} sec)
Real Place	RP = Y(7) Lo/b = Y(7) 1 16 (m)
Real Velocity	RV = Y(10) Lo WO/b = Y(10) 1 1 (10^{5} m/sec)

The electrical currents Y(1), Y(2), Y(1)+Y(2) and the voltage 1-Y(11) are listed as nondimensional values. Time X, voltage U, and the electrical currents Y(1) and Y(2) are moved to a plotter-storage-array which is called at the end of the MAIN PROGRAM.

After each integration, a control statement is called which is specified by the parameter KKX STEP 1 is terminated by means of one of these control statements when the plasma has reached the end of the coaxial accelerator, that means RP = VK(5).

The initial values for STEP 2 are defined at the end of STEP 1. V2 represents equation (49), Y(8) and Y(9), the current derivatives, are determined by equations (55) and (56) in SUBROUTINE FCT2, DERY(3) and DERY(5) are the functions for the decreasing inductance and resistance introduced in equations (64) and (65). DERY(8) and DERY(9) are defined by equations (30), (31), (46) and (47). The integration of STEP 2 is continued until the plasma reaches the end of the compressor coil; RP is then equal to or greater than VK(4)

After termination of STEP 2, SUBROUTINE OUTP initializes the integration of the equation system given in SUBROUTINE FCT3 The initial values for Y(8) and Y(9) are obtained from equation (58) DERY(8) and DERY(9) in SUBROUTINE FCT3 correspond to equations (30) and (31), with DERY(3) = DERY(4) = DERY(5) = 0. This system is integrated as long as the first derivative Y(8) of the compressor coil current is negative. The integration of STEP 3 is terminated by the change of the sign of Y(8)

The integration of STEP 4 begins with the initial values for Y(8) and Y(9), which are obtained by equations (28) and (29). The system of equations in SUBROUTINE FCT4 is the same as in SUBROUTINE FCT3. The integration is continued until the independent variable X has reached the upper bound of the integration interval which was specified in the first section of the MAIN PROGRAM

C. Example of Calculations

The computer program described in this section may be used to investigate the influence of different parameters on the equivalent circuit representing the coaxial accelerator and attached compressor coil One of the parameters which can be varied is the coefficient K7 which is defined in equation (56). The parameter K7 represents the energy stored in the capacitor bank In Figure 21 the curves for the nondimensional capacitor bank voltage U/U_0, the compressor coil current X1, and the coaxial accelerator current X2 are shown. The corresponding values of the variables at T = 0 and the parameters are listed in Table 3, and K7 = VK7 is varied as follows

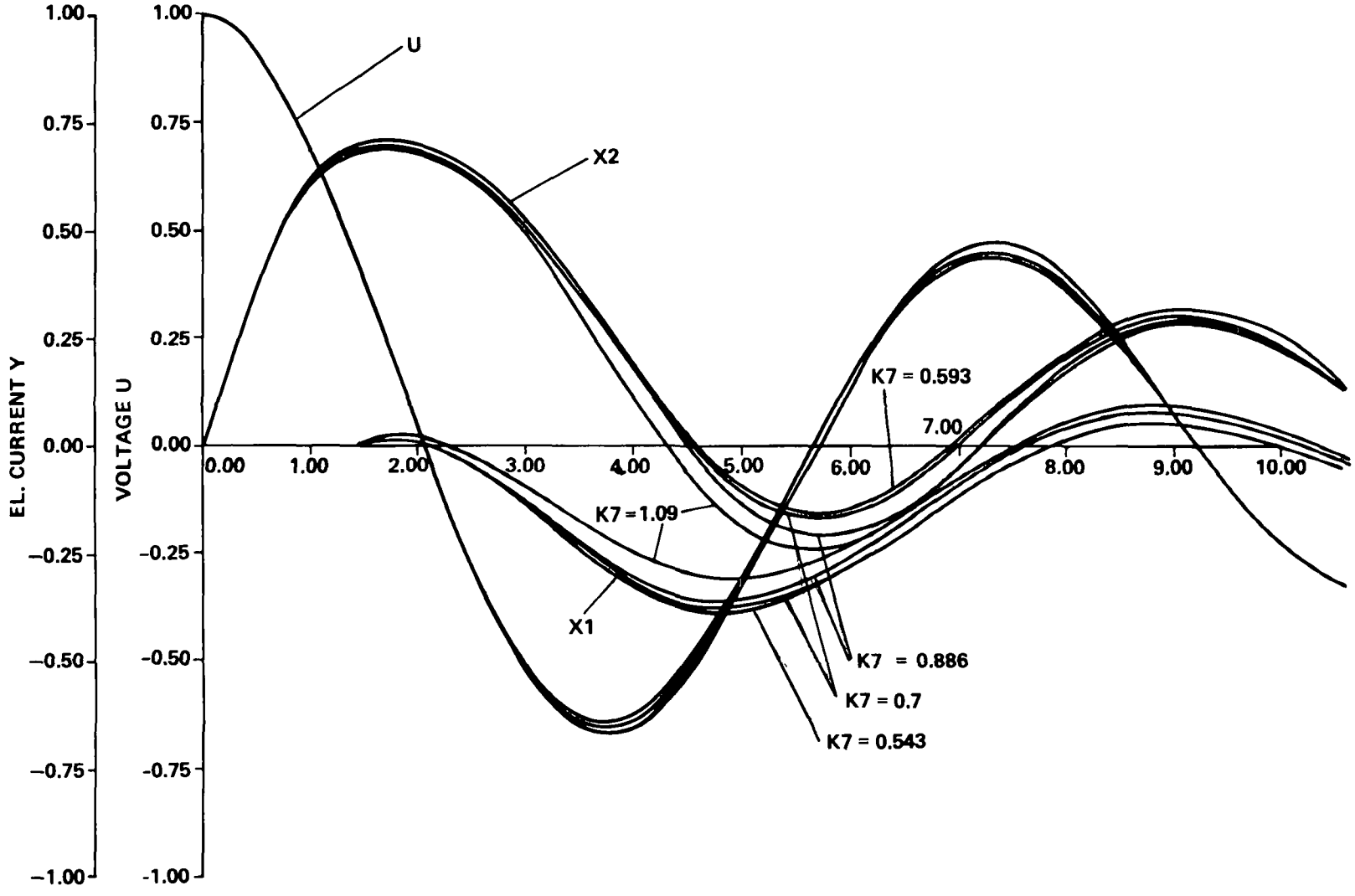

Figure 21 Voltage and current curves for different values of the constant K7

VK7 = 0.543 = 14 KV

VK7 = 0 7 = 16 KV

VK7 = 0.886 = 18 KV

VK7 = 1.09 = 20 KV

The value of VK7 was varied since VK7 $\sim U_0$, as shown in equation (77). Figure 21 shows that the compressor coil current X1 decreases as K7 increases if all other parameters are held constant.

Finally, Figure 22 shows the variation of X1, X2 and U with the plasma resistance X5. The current X1 increases if all other parameters have the value shown in Table 3.

VII. CONCLUSION

The experimental results show that a coaxial accelerator with a compressor coil produces a high density plasma, which can be used to accelerate glass particles for micrometeoroid simulation The discharge of energy stored in the capacitor bank can be investigated theoretically with an equivalent circuit. The theoretical and experimental curves for the electrical current flowing in the coaxial accelerator and in the compressor coil agree within the accuracy of the theoretical approach and the measured values for the equivalent circuit components The photographs of the compressor coil flow and the particle acceleration, together with the high velocities obtained, indicate that the compressor coil confines the plasma during the time when the compressor coil current is increasing

George C. Marshall Space Flight Center
National Aeronautics and Space Administration
Marshall Space Flight Center, Alabama, July 1974
502-21-28-0000

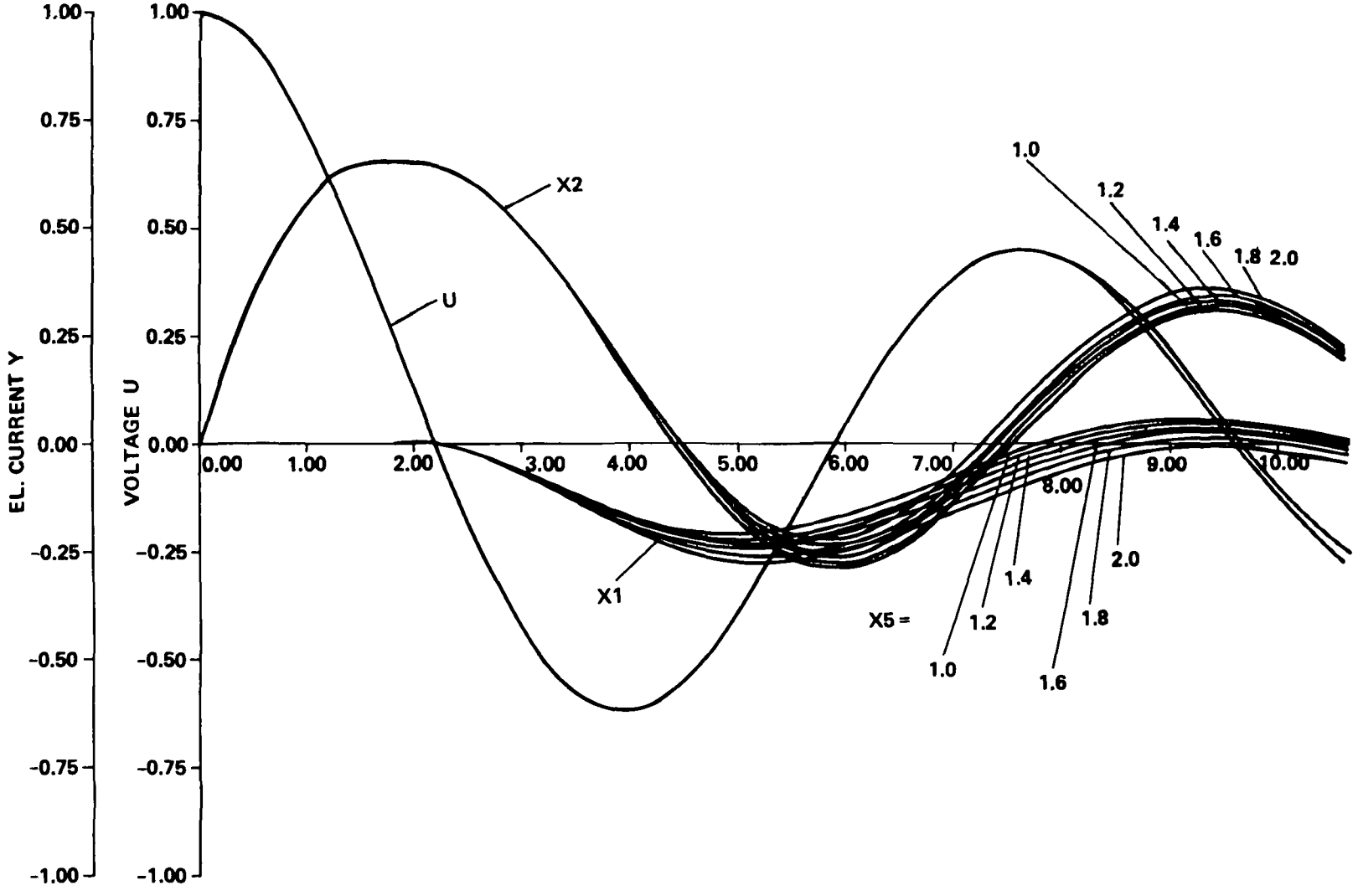

Figure 22. Voltage and current curves for different values of the plasma resistance X5

Page intentionally left blank

Page intentionally left blank

APPENDIX

COMPUTER PROGRAM LISTING

Page intentionally left blank

Page intentionally left blank

```
C      PROGRAM HYPERV
C      --------------
C
C      INTEGRATION BY 4 STEPS
C
       COMMON KKX,V1,V2,V3,V4,V5,U4,W1,W2,W5
       COMMON VK(8)
       COMMON IND,TPLOT(300),UPLOT(300),Y1PLOT(300),Y2PLOT(300)
       DIMENSION Y(11),DERY(11),PRMT(5),AUX(16,11)
C
C      DATA-INPUT
C
C      CONSTANTS
       VK(1)=0.5
       VK(2)=0.999
       VK(4)=0.27
       VK(5)=0.14
C      VK(7)=....
C
C      INITIAL VALUES (STEP1)
       X=0.0
       Y(1)=0.0
       Y(2)=0.0
C      Y(3)=....
C      Y(4)=....
C      Y(5)=....
C
       READ (5,1) VK(7),Y(3),Y(4),Y(5)
     1 FORMAT (4(F10.4))
       Y(6)=0.2
       Y(7)=0.0
       Y(8)=0.0
       Y(9)=1./(1.+2.*Y(4))
       Y(10)=0.0
       Y(11)=0.0
C
C      OUTPUT-FORMATS
C
       WRITE (6,4)
       WRITE (6,5) (Y(I),I=1,7)
       WRITE (6,6)
       WRITE (6,7) (Y(I),I=8,11)
       WRITE (6,8)
       WRITE (6,9) VK(1),VK(2),VK(4),VK(5),VK(7)
       WRITE (6,11)
       WRITE (6,12)
       WRITE (6,17)
C
     4 FORMAT(1H1///,2X,29HINITIAL VALUES AND CONSTANTS:,/,2X,29H--------
      1----------,///,5X,4HY(1),8X,4HY(2),8X,4HY(3),8X,4HY(4),
      28X,4HY(5),8X,4HY(6),8X,4HY(7))
     5 FORMAT (7(2X,E10.3))
     6 FORMAT (/,5X,4HY(8),8X,4HY(9),8X,5HY(10),7X,5HY(11))
     7 FORMAT (4(2X,E10.3))
     8 FORMAT (/,5X,5HVK(1),7X,5HVK(2),7X,5HVK(4),7X,5HVK(5),7X,5HVK(7))
     9 FORMAT (5(2X,E10.3))
    11 FORMAT (////,2X,6HSTEP1:)
    12 FORMAT (2X,6H------)
    17 FORMAT(//,4X,5HT (R),8X,4HY(1),8X,4HY(2),6X,9HY(1)+Y(2),5X,4HY(7),
      18X,5HY(10),6X,7H1-Y(11),/)
```

```
C
C
C     THE DIFFERENTIAL EQUATIONS ARE INTEGRATED BY SUBROUTINE HPCG
C
C     NUMBER OF DIFF. EQUATIONS
      NDIM=11
C
C     LOWER BOUND OF THE INTERVAL
      PRMT(1)=0.
C
C     UPPER BOUND OF THE INTERVAL
      PRMT(2)=10.
C
C     INITIAL INCREMENT OF THE INDEPENDENT VARIABLE X
      PRMT(3)=0.05
C
C     UPPER ERROR BOUND
      PRMT(4)=1.0E-03
C
C     SUBROUTINES CALLED BY SUBROUTINE HPCG
      EXTERNAL OUTP
      EXTERNAL FCT1
      EXTERNAL FCT2
      EXTERNAL FCT3
      EXTERNAL FCT4
C
      CORE=Y(3)
C
C     ERROR WEIGHTS
      DO 20 I=1,11
   20 DERY(I)=1.0/11.0
C
C     PLOTTER-INDEX: IND
      IND=1
C
C     INTEGRATION STEP1
C     -----------------
      CALL HPCG (PRMT,Y,DERY,NDIM,IHLF,FCT1,OUTP,AUX)
C     END  INTEGRATION STEP1
C
      WRITE (6,13)
   13 FORMAT (//,2X,6HSTEP2:)
      WRITE (6,12)
      WRITE (6,17)
C
C     INITIAL VALUES (STEP2) ARE DEFINED AT THE END OF STEP1
      X=PRMT(1)
      V1=X
      V2=(VK(4)-VK(5))/Y(10)
      V3=Y(3)
      V4=Y(4)
      V5=Y(5)
      Y(8)=Y(4)*(1.-Y(11)-Y(6)*Y(2))/(Y(3)+Y(4)+Y(3)*Y(4))
      Y(9)=Y(3)*(1.-Y(11)-Y(6)*Y(2))/(Y(3)+Y(4)+Y(3)*Y(4))
C
C     ERROR WEIGHTS
      DO 21 I=1,11
   21 DERY(I)=1.0/11.0
C
C     INTEGRATION STEP2
```

```
C      ----------------
       CALL HPCG (PRMT,Y,DERY,NDIM,IHLF,FCT2,OUTP,AUX)
C      END INTEGRATION STEP2
C
       WRITE (6,14)
   14  FORMAT (//,2X,6HSTEP3:)
       WRITE (6,12)
       WRITE (6,17)
C
C      INITIAL VALUES (STEP3) ARE DEFINED AT THE END OF STEP2
       X=PRMT(1)
       Y(8)=(Y(4)*(1.0-Y(11)-Y(6)*(Y(1)+Y(2)))-(1.0+Y(4))*Y(5)*Y(1))/(Y(3
      1)+Y(4)+Y(3)*Y(4))
       Y(9)=(Y(3)*(1.0-Y(11)-Y(6)*(Y(1)+Y(2)))+Y(5)*Y(1))/(Y(3)+Y(4)+Y(3)
      1*Y(4))
C
C      ERROR WEIGHTS
       DO 22 I=1,11
   22  DERY(I)=1.0/11.0
C
C      INTEGRATION STEP3
C      ----------------
       CALL HPCG (PRMT,Y,DERY,NDIM,IHLF,FCT3,OUTP,AUX)
C      END INTEGRATION STEP3
C
       WRITE (6,15)
   15  FORMAT (//,2X,6HSTEP4:)
       WRITE (6,12)
       WRITE (6,17)
C
C      INITIAL VALUES (STEP4) ARE DEFINED AT THE END OF STEP3
       X=PRMT(1)
       Y(3)=CORE
       Y(8)=(Y(4)*(1.0-Y(11)-Y(6)*(Y(1)+Y(2)))-(1.0+Y(4))*Y(5)*Y(1))/(Y(3
      1)+Y(4)+Y(3)*Y(4))
       Y(9)=(Y(3)*(1.0-Y(11)-Y(6)*(Y(1)+Y(2)))+Y(5)*Y(1))/(Y(3)+Y(4)+Y(3)
      1*Y(4))
C
C      ERROR WEIGHTS
       DO 23 I=1,11
   23  DERY(I)=1.0/11.0
C
C      INTEGRATION STEP4
C      ----------------
       CALL HPCG (PRMT, Y,DERY,NDIM,IHLF,FCT4,OUTP,AUX)
C      END INTEGRATION STEP4
C
       WRITE (6,16)
   16  FORMAT (////)
C
C      PLOT-PROGRAM  BEGIN     (BENSON-PLOTTER)
C      ------------------
C
C      PLOTTER-SCALE-FACTORS
       TPLOT(IND)=0.0
       TPLOT(IND+1)=1.0
       UPLOT(IND)=-1.0
       UPLOT(IND+1)=0.25
       Y1PLOT(IND)=-1.0
       Y1PLOT(IND+1)=0.25
```

```
      Y2PLOT(IND)=-1.0
      Y2PLOT(IND+1)=0.25
C
      CALL PLOT(10.,7.,-3)
      CALL FACTOR(2.0)
      CALL AXIS(0.,4.,6HTIME T,-6,10.,0.,TPLOT(IND),TPLOT(IND+1))
      CALL AXIS(0.,0.,9HVOLTAGE U,9,8.,90.,UPLOT(IND),UPLOT(IND+1))
      CALL AXIS(-1.,0.,12HEL.CURRENT Y,12,8.,90.,Y1PLOT(IND),Y1PLOT(IND+
     11))
      CALL LINE(TPLOT(1),UPLOT(1),IND-1,1,10,1)
      CALL LINE(TPLOT(1),Y1PLOT(1),IND-1,1,0,1)
      CALL LINE(TPLOT(1),Y2PLOT(1),IND-1,1,10,2)
C
      CALL SYMBOL(0.2,2.0,0.21,11HHYPERV-HPCG,0.0,11)
      CALL SYMBOL(0.2,1.5,0.14,5HU     ,0.0,5)
      CALL SYMBOL(999.,999.,0.08,1,0.0,-1)
      CALL SYMBOL(0.2,1.2,0.14,5HY(1)  ,0.0,5)
      CALL SYMBOL(999.,999.,0.14,1H-,0.0,1)
      CALL SYMBOL(0.2,0.9,0.14,5HY(2)  ,0.0,5)
      CALL SYMBOL(999.,999.,0.08,2,0.0,-1)
C
      CALL PLOT(14.,0.,-3)
      CALL FACTOR(1.0)
      CALL PLOT(0.0,-7.0,-3)
      CALL PLOT(0.,0.,4)
      STOP
C
C     PLOT-PROGRAM  END
C
      END
C
      SUBROUTINE HPCG (PRMT,Y,DERY,NDIM,IHLF,FCT,OUTP,AUX)
C     ----------------------------------------------------
C
      SUBROUTINE OUTP (X,Y,DERY,IHLF,NDIM,PRMT)
C     -----------------------------------------
C
      COMMON KKX,V1,V2,V3,V4,V5,U4,W1,W2,W5
      COMMON VK(8)
      COMMON IND,TPLOT(300),UPLOT(300),Y1PLOT(300),Y2PLOT(300)
      DIMENSION Y(11),DERY(11),PRMT(5)
C
      SS=Y(1)+Y(2)
      U=1.0-Y(11)
      RT=X*1.06
      RP=Y(7)*1.16
      RV=Y(10)*1.1
      PRMT(1)=X
C
      UPLOT(IND)=U
      TPLOT(IND)=RT
      Y1PLOT(IND)=Y(1)
      Y2PLOT(IND)=Y(2)
C
      WRITE (6,30) RT,Y(1),Y(2),SS,RP,RV,U
   30 FORMAT (7(2X,E10.4))
      IND=IND+1
C
      GO TO (100,200,300,400),KKX
C
```

```
  100 IF (RP .GE. VK(5)) GO TO 500
      RETURN
  200 IF (RP .GE. VK(4)) GO TO 500
      RETURN
  300 IF (Y(8) .GE. 0.) GO TO 500
      RETURN
  400 RETURN
C
  500 PRMT(5)=1.
      RETURN
      END
C
      SUBROUTINE FCT1 (X,Y,DERY)
C     ----------------------------
C
      COMMON KKX,V1,V2,V3,V4,V5,U4,W1,W2,W5
      COMMON VK(8)
      DIMENSION Y(11),DERY(11)
C
      DERY(1)=0.
      DERY(2)=Y(9)
      DERY(3)=0.
      DERY(4)=Y(10)
      DERY(5)=0.
      DERY(6)=0.
      DERY(7)=Y(10)
      DERY(8)=0.
      DERY(9)=(-Y(2)*(VK(7)*Y(2)*Y(2)+1.)-Y(9)*(Y(6)+2*Y(10)))/(1.+Y(4))
      DERY(10)=VK(7)*Y(2)*Y(2)
      DERY(11)=Y(2)
C
      KKX=1
C
      RETURN
      END
C
      SUBROUTINE FCT2 (X,Y,DERY)
C     ----------------------------
C
      COMMON KKX,V1,V2,V3,V4,V5,U4,W1,W2,W5
      COMMON VK(8)
      DIMENSION Y(11),DERY(11)
C
      DERY(1)=Y(8)
      DERY(2)=Y(9)
      DERY(3)=-VK(1)*V3/V2
      DERY(4)=0.
      DERY(5)=-V5*VK(2)/V2
      DERY(6)=0.
      DERY(7)=Y(10)
      DERY(8)=(-(1.0+Y(4))*(Y(8)*(Y(6)+Y(5)-2*V3*VK(1)/V2)+Y(9)*Y(6)+Y(1
     1)*(1.0-V5*VK(2)/V2)+Y(2))+Y(6)*Y(8)+Y(6)*Y(9)+Y(1)+Y(2))/((1.0+Y(3
     2))*(1.0+Y(4))-1.0)
      DERY(9)=(-(1.0+Y(3))*(Y(6)*Y(8)+Y(6)*Y(9)+Y(1)+Y(2))+Y(8)*(Y(5)+Y(
     16)-2*V3*VK(1)/V2)+Y(6)*Y(9)+Y(1)*(1.0-V5*VK(2)/V2)+Y(2))/((1.0+Y(3
     2))*(1.0+Y(4))-1.0)
      DERY(10)=0.
      DERY(11)=Y(1)+Y(2)
C
      KKX=2
```

```
C
      RETURN
      END
C
      SUBROUTINE FCT3 (X,Y,DERY)
C     ------------------------
C
      COMMON KKX,V1,V2,V3,V4,V5,U4,W1,W2,W5
      COMMON VK(8)
      DIMENSION Y(11),DERY(11)
C
      DERY(1)=Y(8)
      DERY(2)=Y(9)
      DERY(3)=0.
      DERY(4)=0.
      DERY(5)=0.
      DERY(6)=0.
      DERY(7)=Y(10)
      DERY(8)=(-(1.0+Y(4))*(Y(8)*(Y(6)+Y(5))+Y(9)*Y(6)+Y(1)+Y(2))+Y(6)*Y
     1(8)+Y(6)*Y(9)+Y(1)+Y(2))/((1.0+Y(3))*(1.0+Y(4))-1.0)
      DERY(9)=(-(1.0+Y(3))*(Y(6)*Y(8)+Y(6)*Y(9)+Y(1)+Y(2))+Y(8)*(Y(5)+Y(
     16))+Y(6)*Y(9)+Y(1)+Y(2))/((1.0+Y(3))*(1.0+Y(4))-1.0)
      DERY(10)=0.
      DERY(11)=Y(1)+Y(2)
C
      KKX=3
C
      RETURN
      END
C
      SUBROUTINE FCT4 (X,Y,DERY)
C     ------------------------
C
      COMMON KKX,V1,V2,V3,V4,V5,U4,W1,W2,W5
      COMMON VK(8)
      DIMENSION Y(11),DERY(11)
C
      DERY(1)=Y(8)
      DERY(2)=Y(9)
      DERY(3)=0.
      DERY(4)=0.
      DERY(5)=0.
      DERY(6)=0.
      DERY(7)=Y(10)
      DERY(8)=(-(1.0+Y(4))*(Y(8)*(Y(6)+Y(5))+Y(9)*Y(6)+Y(1)+Y(2))+Y(6)*Y
     1(8)+Y(6)*Y(9)+Y(1)+Y(2))/((1.0+Y(3))*(1.0+Y(4))-1.0)
      DERY(9)=(-(1.0+Y(3))*(Y(6)*Y(8)+Y(6)*Y(9)+Y(1)+Y(2))+Y(8)*(Y(5)+Y(
     16))+Y(6)*Y(9)+Y(1)+Y(2))/((1.0+Y(3))*(1.0+Y(4))-1.0)
      DERY(10)=0.
      DERY(11)=Y(1)+Y(2)
C
      KKX=4
      RETURN
      END
```

REFERENCES

1 Baer, P.G., and Smith, H C. Experimental and Theoretical Studies on the Interior Ballistics of Light Gas Guns Sixth Symp. on Hypervelocity Impact, Cleveland, Ohio, Aug 1963

2. Curtis, J.S An Accelerated Reservoir Light-Gas Gun NASA TN D-1144, Feb. 1962

3. Moore, E.T., Mumma, D , Godfrey, C S., and Bernstein, D Explosive Gas Guns for Hypervelocity Acceleration. Fourth Symp on Hypervelocity Techniques, Tullahoma, Tennessee, Nov. 1965

4 Friichtenicht, J F , and Hamermesh, B.: Ballistic Impacts by Microscopic Projectiles Fourth Symp. on Hypervelocity Impact, Eglin AFB, Florida, April 1960

5 Friichtenicht, J.F , Slattery, J C., and Hansen, D O Electrostatic Accelerators – Experimental Techniques Seventh Symp on Hypervelocity Impact, Tampa, Florida, Nov 1964.

6 Scully, C N., and Cowan, P L . Hypervelocity Gun for Micrometeorite Impact Simulation Employing Capacitor Discharge in a Condensed Phase Fourth Symp on Hypervelocity Impact, Tampa, Florida, April 1960

7. Igenbergs, E. Magnetogasdynamische Kompression Eines Plasmas zur Beschleunigung von Teilchen für die Simulation von Mikrometeoriden. Deutsche Luft-und Raumfahrt, Mitteilungen, DLR-MITT 73-15, May 1973.

8. Artsimovitch, L A., et al Electrodynamic Acceleration of Plasma Bunches. Soviet Physics JETP, vol 6, no. 1, January 1958, pp 1-5

9. Rosen, F D A Magnetically Augmented Rail Gun Seventh Symp on Hypervelocity Impact, Tampa, Florida, Nov. 1964.

10 Brast, D E , and Sawle, D R. Study of a Rail-Type MHD Hypervelocity Accelerator. Seventh Symp on Hypervelocity Impact, Tampa, Florida, Nov 1964

11. Shriver, E.L Analytical and Experimental Investigation of the Coaxial Plasma Gun For Use as a Particle Accelerator NASA TN D-6687, April 1972.

"The aeronautical and space activities of the United States shall be conducted so as to contribute . . to the expansion of human knowledge of phenomena in the atmosphere and space The Administration shall provide for the widest practicable and appropriate dissemination of information concerning its activities and the results thereof"

—NATIONAL AERONAUTICS AND SPACE ACT OF 1958

NASA SCIENTIFIC AND TECHNICAL PUBLICATIONS

TECHNICAL REPORTS Scientific and technical information considered important, complete, and a lasting contribution to existing knowledge

TECHNICAL NOTES Information less broad in scope but nevertheless of importance as a contribution to existing knowledge

TECHNICAL MEMORANDUMS Information receiving limited distribution because of preliminary data, security classification, or other reasons Also includes conference proceedings with either limited or unlimited distribution.

CONTRACTOR REPORTS Scientific and technical information generated under a NASA contract or grant and considered an important contribution to existing knowledge

TECHNICAL TRANSLATIONS Information published in a foreign language considered to merit NASA distribution in English

SPECIAL PUBLICATIONS Information derived from or of value to NASA activities Publications include final reports of major projects, monographs, data compilations, handbooks, sourcebooks, and special bibliographies

TECHNOLOGY UTILIZATION PUBLICATIONS Information on technology used by NASA that may be of particular interest in commercial and other non-aerospace applications Publications include Tech Briefs, Technology Utilization Reports and Technology Surveys

Details on the availability of these publications may be obtained from:

SCIENTIFIC AND TECHNICAL INFORMATION OFFICE

NATIONAL AERONAUTICS AND SPACE ADMINISTRATION

Washington, D.C. 20546